Evaluation of the WRF-solar model for 72-hour ahead forecasts of global horizontal irradiance in West Africa: a case study for Ghana

Windmanagda Sawadogo, Benjamin Fersch, Jan Bliefernicht, Stefanie Meilinger, Thomas Rummler, Seyni Salack, Samuel Guug, Harald Kunstmann

Angaben zur Veröffentlichung / Publication details:

Sawadogo, Windmanagda, Benjamin Fersch, Jan Bliefernicht, Stefanie Meilinger, Thomas Rummler, Seyni Salack, Samuel Guug, and Harald Kunstmann. 2024. "Evaluation of the WRF-solar model for 72-hour ahead forecasts of global horizontal irradiance in West Africa: a case study for Ghana." *Solar Energy* 271: 112413. https://doi.org/10.1016/j.solener.2024.112413.

Solar Energy 271 (2024) 112413

Contents lists available at ScienceDirect

Solar Energy

journal homepage: www.elsevier.com/locate/solener

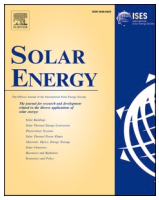

Evaluation of the WRF-solar model for 72-hour ahead forecasts of global horizontal irradiance in West Africa: A case study for Ghana

Windmanagda Sawadogo [a,*], Benjamin Fersch [b], Jan Bliefernicht [a], Stefanie Meilinger [c], Thomas Rummler [a], Seyni Salack [d], Samuel Guug [d], Harald Kunstmann [a,b,*]

[a] Institute of Geography, University of Augsburg, 86159 Augsburg, Germany
[b] Campus Alpin, Institute of Meteorology and Climate Research (IMK-IFU), Karlsruhe Institute of Technology, 82467 Garmisch-Partenkirchen, Germany
[c] International Centre for Sustainable Development (IZNE), University of Applied Sciences Bonn-Rhein-Sieg, 53757 Sankt Augustin, Germany
[d] West African Science Service Centre on Climate Change and Adapted Land Use (WASCAL) Competence Centre, Ouagadougou, Burkina Faso

ARTICLE INFO

Keywords:
WRF-Solar
Global horizontal irradiance
Forecasting
West Africa
Ghana

ABSTRACT

Accurate global horizontal irradiance (GHI) forecasting is critical for integrating solar energy into the power grid and operating solar power plants. The Weather Research and Forecasting model with its solar radiation extension (WRF-Solar) has been used to forecast solar irradiance in different regions around the world. However, the application of the WRF-Solar model to the prediction of GHI in West Africa, particularly Ghana, has not yet been investigated. The aim of this study is to evaluate the performance of the WRF-Solar model for predicting GHI in Ghana, focusing on three automatic weather stations (Akwatia, Kumasi and Kologo) for the year 2021. We used two one-way nested domains (D1 = 15 km and D2 = 3 km) to investigate the ability of the fully coupled WRF-Solar model to forecast GHI up to 72-hour ahead under different atmospheric conditions. The initial and lateral boundary conditions were taken from the ECMWF high-resolution operational forecasts. Our findings reveal that the WRF-Solar model performs better under clear skies than cloudy skies. Under clear skies, Kologo performed best in predicting 72-hour GHI, with a first day nRMSE of 9.62 %. However, forecasting GHI under cloudy skies at all three sites had significant uncertainties. Additionally, WRF-Solar model is able to reproduce the observed GHI diurnal cycle under high AOD conditions in most of the selected days. This study enhances the understanding of the WRF-Solar model's capabilities and limitations for GHI forecasting in West Africa, particularly in Ghana. The findings provide valuable information for stakeholders involved in solar energy generation and grid integration towards optimized management in the region.

1. Introduction

Energy in all forms is critical to the running of any nation's socio-economic activities. About 81 % of global energy generation comes from fossil fuels (IEA, 2021). With the rising demand for energy and the specific targets of the Paris Agreement, there is an urgent need to reduce dependence on fossil fuels [45]. Renewable energy such as solar energy has become a viable alternative to conventional forms of energy due to its low cost [33]. Over the last decade, solar photovoltaic (PV) technologies have been part of the energy mix in many West African countries, particularly in Ghana. Potentially high solar resources make Ghana a suitable location for developing robust solar energy projects for off-grid and grid-connected systems [24]. However, solar irradiance shows a strong seasonal variability in this country with reduced solar resources during the rainy season and Harmattan dust storm period [52].

Solar energy forecasting can play a significant role in the operational efficiency of solar power plants and their integration into the electricity grid[36,1]. Global horizontal irradiance (GHI) is one of the most important meteorological variables for assessing the potential of PV, as it helps to determine the amount of solar energy that can be generated at a specific location over a given forecast horizon[43]. Various methods are used for GHI forecasting and they can be classified into physical (dynamical) approaches and statistical approaches. Both approaches have their advantages and limitations, and their choice depends on data availability, computational resources and other issues[71]. Statistical approaches can be based on machine learning (ML) algorithms and rely on historical observations for GHI forecasting [57], while physical

* Corresponding authors.
E-mail addresses: windmanagda.sawadogo@uni-a.de (W. Sawadogo), harald.kunstmann@kit.edu (H. Kunstmann).

https://doi.org/10.1016/j.solener.2024.112413
Received 5 June 2023; Received in revised form 7 February 2024; Accepted 15 February 2024
Available online 1 March 2024

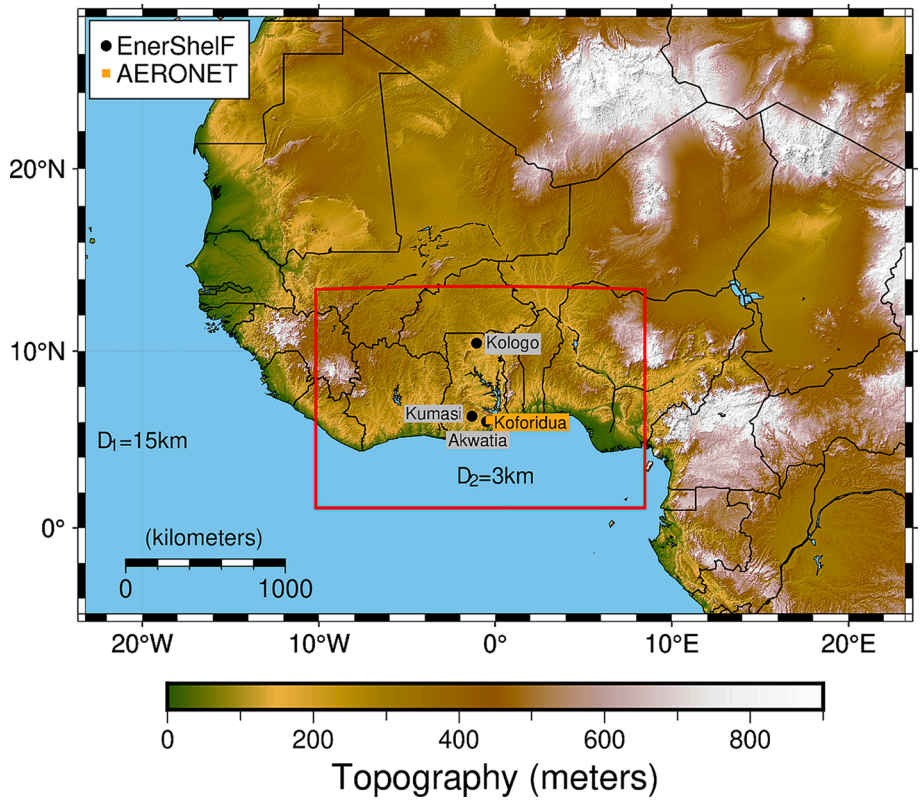

Fig. 1. The WRF-Solar domain setup. Colors represent the model topography in meters. The red square denotes the inner domain (D2 = 3 km), while the outer domain (D1 = 15 km) encompasses the area outside this square. The black dots indicate the locations of the EnerShelF automatic weather stations (Akwatia, Kumasi, and Kologo). Additionally, the orange square marks the AERONET station in Koforidua. (For interpretation of the references to colour in this figure legend, the reader is referred to the web version of this article.)

approaches, such as numerical weather prediction (NWP) models, are based on physical equations to forecast GHI several hours or days in ahead[58,79,46]. The solar energy version of the Weather Research and Forecasting (WRF) model (WRF-Solar) is a numerical weather prediction model designed specifically for the solar energy industry. The model is widely used for GHI forecasting due to its ability to provide high-resolution and accurate forecasts. In addition, the WRF-Solar model is able to provide forecasts for different time periods (e.g., sub-hourly, or daily) in high spatial resolution, which is useful for various solar energy applications[31].

The WRF-Solar model is a valuable tool for GHI forecasting due to its ability to account for the effects of cloud cover, atmospheric water vapor, and aerosols on GHI values[31]. The model has been applied to GHI forecasting in various regions and has demonstrated improved accuracy compared to traditional GHI forecasting models. A study by Sosa-Tinoco et al. [67] compared the WRF-Solar model against observations from ground-based meteorological stations located in two major solar plants in Spain and India. They found that the model could reproduce the observed meteorological conditions of the solar radiation components with reasonable accuracy for the first and second-day forecast and demonstrated its potential for use in managing and optimizing of solar energy systems. Another study by Gueymard and Jimenez [23] evaluated the performance of the WRF-Solar model in forecasting the day-ahead GHI for the desert area at Shagaya, Kuwait and found that the model performed better under clear skies than under cloudy skies. [30,32] demonstrated the performance of WRF-Solar in forecasting GHI across the United States. Lee et al. [38] analyzed the performance of different nowcasting methods for forecasting GHI in real-time and evaluated their accuracy near Sacramento, California. Their results show that the WRF-Solar model was able to accurately forecast GHI under different atmospheric conditions.

On the other hand, statistical approaches such as ML models were more reliable in forecasting GHI than NWP models for lead times up to 6 h [72]. In Africa, most GHI forecasts are based on the ML models. A study by Mutavhatsindi et al. [51] showed that an ML algorithm based on long-term memory (LSTM) networks achieved high accuracy for GHI forecasting for Pretoria, while another study by Mpfumali et al. [49] found that quantile regression was most effective for Cape Town. Chaaraoui et al. [7] used ML techniques for short-term forecasts of solar irradiance using an all-sky camera in Ghana. Other statistical methods such as Gaussian process regression, genetic algorithm and different ML models have also been used for GHI forecasting in Africa [59,8,78]. However, the models from ML have drawbacks, including limited short-term forecasting (less than 24 h) and a narrow subset of meteorological data[65]. Moreover, ML models are highly dependent on the availability of accurate historical observations. They may not be suitable for sites with limited data or significant changes in weather patterns. For instance, the West Africa region has limited long-term observational time series and is characterized by complex and challenging weather patterns, such as dust storms and rapid fluctuations of cloud cover[53], which can negatively impact the performance of ML models[69]. Yet, the ML models may capture the general trend but fail to capture quick variations of GHI values[70]. Additionally, ML model methods have been found to have limited performance in terms of GHI day-ahead forecasting compared to NWP such as the WRF model[11,38].

To date, there is limited information on the performance of the WRF-Solar model in GHI forecasting in West Africa, even in Africa. Further research is needed to fully exploit the potential of the WRF-Solar model in GHI forecasting in West Africa and to further improve its accuracy. Therefore, this study investigates the performance of the state-of-the-art WRF-Solar model for 72-hour GHI forecasting in West Africa, particularly in Ghana for 1-hour temporal resolution and 3 km spatial

Fig. 2. Operational automatic weather stations (AWS) in the courtyard of three health centers in Ghana. Panel (a) shows the AWS at Saint Michael Hospital in Kumasi, panel (b) the AWS at Kologo Health Centre in Kologo and panel (c) the AWS at Saint Dominic Hospital in Akwatia.

resolution. The direct effect of aerosol is considered in this study as suggested by Sawadogo et al. [62] who showed that considering time-varying aerosol properties in the WRF-Solar model improves simulated GHI values for the region. Moreover, the 72-hour GHI forecasting are evaluated against ground observations from three novel automatic weather stations (AWS) using various statistical performance measures under different atmospheric conditions. The stations were implemented at three different health centres over Ghana as part of the EnerShelF (Energy Supply for Healthcare Facilities) project. One of the key objectives of this project is to provide operational GHI forecast data for the three health center sites to improve PV-based energy solutions at these centers.

The paper is structured as follows: The next section presents the description and configuration of the WRF-Solar model, as well as the study area, and the methodology. Section 3 provides the results and discussion of the evaluation of the model under clear-sky, cloudy sky, and all-sky conditions. Finally, the last section presents the main findings and conclusions of the study.

2. Data and methodology

2.1. Study area

This study focuses on three locations, namely Akwatia, Kumasi and Kologo, in Ghana, West Africa (Fig. 1). Ghana is characterized by three climatic zones (Costal, Guinean Forest and Savannah) as defined by[4]. The sites of Akwatia and Kumasi belong to the Forest zone located in the southern part of Ghana. This zone has a tropical rainforest climate and is usually cloudy with stratiform type clouds associated with persistent rainfall [34]. There are two rainy seasons in this zone, the first from April to July and the second from September to November. The Savannah zone (Kologo) is located in the northern part of Ghana and characterized by a hot and dry climate. In this zone, it is mostly clear in the dry season. During the rainy season, clouds are of the cumulus type, which are associated with thunderstorms and strong rainfall events. The region has a rainy season from May to September with a peak in August.

2.2. Data

2.2.1. Automatic weather stations (AWS)

We collected high-quality GHI for 2021 from three AWS as part of the EnerShelF project (https://www.enershelf.de) in Ghana, coordinated by the University of Applied Sciences Bonn-Rhine-Sieg (H-BRS). These stations were installed in late September 2020 by a joint team from the University of Augsburg (UniA), Germany, the West African Science Service Centre on Climate Change and Adapted Land Use (WASCAL), and the Ghana Meteorological Agency (GMet). The AWS are located at three different health centers: Saint Dominic Hospital (Akwatia), Saint Michael Hospital (Kumasi) and Kologo Health Center (Kologo). Fig. 2 shows the AWS installed in the courtyard of the different health centers. The AWS measure various meteorological variables such as GHI, precipitation, relative humidity, air temperature at 2 m above ground level, soil temperature at different depths (5, 20 and 50 cm), surface pressure, wind speed and direction using the same measurement equipment. The data is recorded with an average five-minute interval. Main maintenance, usually every six months, consists of replacing defective batteries, cleaning or/and replacing different broken sensors, recalibrating the data logger in case of incorrect settings, and keeping the area (vegetation) around the stations clear to avoid any shading. Additionally, there is trained personnel at the different sites to clean the solar radiation sensors at night in case of dust events and other basis maintenance issues. The raw data is post-processed, and initial quality controlled by UniA and then upload to the WADI (WASCAL Data Infrastructures, https://www.wascal-dataportal.org) database for consumption by the end users of the project.

2.2.2. AERONET

The AERONET (AErosol RObotic NETwork) is a global network for ground-based measurement of atmospheric aerosols using the sun photometry [26]. The network was established in the early 1990′s and currently comprises about 1315 measurement sites scattered worldwide. AERONET provides various microphysical properties of aerosols such as size distribution, composition, and optical depth at different wavelengths. About 16 sun photometer measurements have been installed in West Africa, of which Niger has the highest number (4). Ghana has only one site, Koforidua, located within our domain (see Fig. 1). The main campus of the All-Nations University houses the device on the roof of a building about 5 km from the center of Koforidua. From the AERONET platform, we retrieve the daily aerosol optical depth (AOD) level 2.0 (high-quality data) at 440 nm and also the Ånsgtröm exponent (AE) at 440–675 nm values for 2021. The AOD at 550 nm (AOD_{550}) was calculated using the equation of [66]:

$$AE = \frac{-log\frac{\tau_{\lambda_1}}{\tau_{\lambda_2}}}{log\frac{\lambda_1}{\lambda_2}} \quad (1)$$

where τ_{λ_1} and τ_{λ_2} is the total AOD at wavelength λ_1 and λ_2 respectively.

2.2.3. Observational total cloud cover

Clouds are an important parameter in GHI forecasting that remains one of the uncertainties in climate models. For a deeper analysis of the WRF-Solar GHI forecasting, we also evaluated the model's fractional cloud cover (CFC) forecasting with satellite data. We used CFC from the Interim Climate Data Record (ICDR) SEVIRI (Spinning Enhanced Visible and InfraRed Imager) instrument on board the Meteosat Second Generation (MSG) satellites [18]. The SEVIRI on MSG uses the CLAAS-2 (CLoud property dAtAset using SEVIRI, Edition 2) algorithm to estimate clouds, providing an accurate and reliable estimation of cloud properties [3]. Daily and monthly mean values are available from 2018 on with a spatial resolution of about 5 km. For this study, we retrieved the daily CFC data from the website CM SAF (EUMETSAT Satellite Application Facility on Climate Monitoring)..

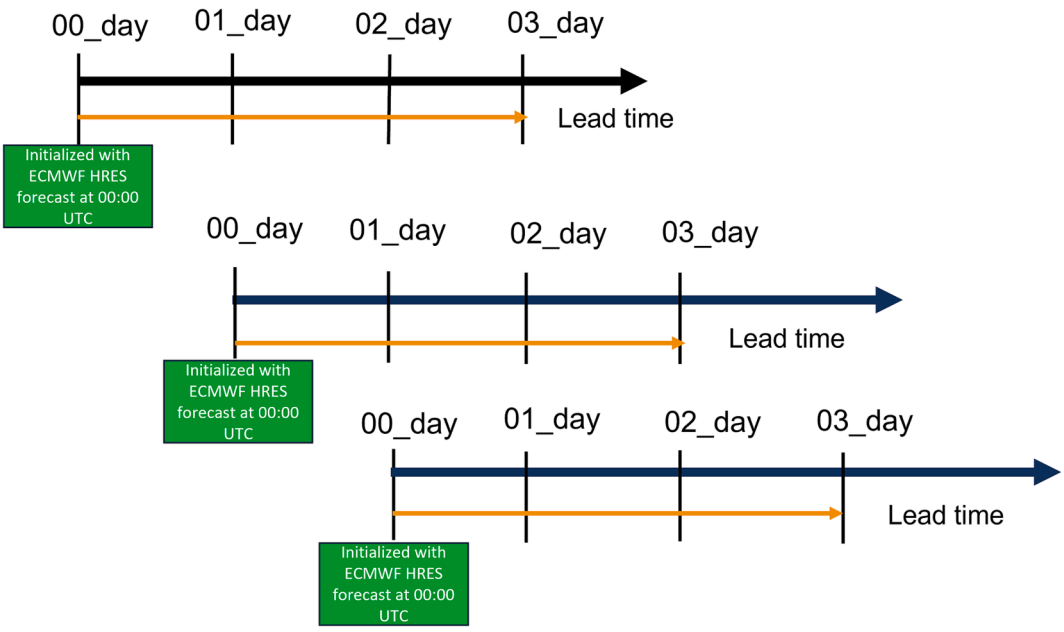

Fig. 3. Exemplary forecast cycle. Each day, the model is initialized with the ECWMF-HRES at 00 UTC. The forecast starts on the first day, denoted as 00_day and ends at 03_day (00 UTC). 01_day indicates the second day of the forecast, while 02_day is the third day of the forecast.

2.2.4. *Copernicus atmosphere Monitoring Service (CAMS)*

Copernicus Atmosphere Monitoring Service (CAMS) data use the Integrated Forecasting System (IFS) of the European Centre for Medium-Range Weather Forecasts (ECMWF) and enable near real-time forecasting and reanalysis of aerosols. IFS uses 4D-VAR, a four-dimensional variational data assimilation technique, to incorporate various meteorological observations and satellite-based atmospheric composition queries [28]. Twice daily (at 00:00 UTC and 12:00 UTC), forecasts are produced for aerosols and chemical substances for the next five days. The forecast includes 56 reactive trace gases in the troposphere and stratospheric ozone. It also provides information on seven different types of aerosols, including desert dust, sea salt, organic matter, black carbon, sulphate, and nitrate and ammonium [15]. The CAMS has a horizontal spectral resolution of TL511 (~40 km) with 137 vertical levels from 0.01 to 1013 hPa. The forecast data are available in a 3-hour temporal resolution from 2015 on. We retrieved 72-hour forecast of AOD for 2021 at different wavelengths: 469, 550, and 865 nm with the initialized time at 00:00 UTC and then calculated the AE using Eq. (1). We also retrieved 3 hourly AOD_{550} reanalysis data from CAMS for comparison with the AERONET data at Koforidua for 2021. This comparison aims to see how well the CAMS data simulate the AOD_{550} at Koforidua and the confidence of using the data in this study.

2.2.5. *ECWMF-HRES*

ECMWF is a pioneering organization in the field of weather forecasting, providing global weather forecast information [16]. The forecasts are continuously refined by updating the models with the latest observational data from satellites, weather balloons and other sources. The ECMWF offers different types of forecasts. For this study, we used the high-resolution forecast (HRES) data. HRES are produced using advanced NWP models that consider a large number of atmospheric variables and use high-resolution computational grids to produce comprehensive weather forecasts with a single prediction. HRES is ECMWF's most accurate prediction of the weather forecast. In addition, with the updated IFS and its new operating cycle (45r1), HRES provides a more accurate forecast compared to the 43r3 cycle, especially in the tropics [25], such as the West Africa region. The forecast is produced twice daily based on observations at 00 and 12 UTC and ranges from the first day to 10 days ahead with a temporal resolution of 3 h. The HRES has an interpolated grid of about 9 km with 137 vertical levels and the pressure at the top of the model is about 0.01 hPa. We have obtained 3-hourly data for 72-hour forecasts at 00 UTC (initialization time) for all the necessary variables (surface and pressure level) required to drive WRF-Solar for the year 2021 from the ECMWF website.

2.3. *WRF-solar modeling*

The WRF-Solar configuration is specifically designed for forecasting of solar energy applications. For this study, we used WRF-Solar version 4.2.1, with two one-way nested domains over West Africa. The optimized WRF-Solar for West Africa is highlighted by Sawadogo et al. [62]. To ensure consistency with the optimized study, we used the same domains and configurations for the GHI forecasting. The outer domain (D1) has a spatial resolution of 15 km and extends from 5°S to 30°N and from 23°W to 23°E, with 299x219 grid points. The inner domain (D2) covers a smaller area, from 1°N to 14.5°N and from 10°W to 8.5°E, with a higher resolution of 3 km and 600x400 grid points (as shown in Fig. 1). In the WRF Preprocessing System (WPS), the land use information was obtained from the 21-class Moderate Resolution Imaging Spectroradiometer (MODIS) land use index and fraction, and the green vegetation index from the Fraction of Photosynthetically Active Radiation (FPAR). To initialize the land use in the model, we used the GEODATA TOPO 10 M United States Geological Survey (USGS) topography data. For the initial and lateral boundary conditions (LBC) of the model, we used the forecast data from ECMWF-HRES. For each day, the model was initialized at 00 UTC using the data from ECWMF-HRES and the forecast was produced up to 3 days ahead for the year 2021 (from 01-January to 31-December). Fig. 3 shows the flow of the forecast. Each forecast begins at 00 UTC (initialization time) and ends at 03_day (00 UTC). 00_day denotes the first day of the forecast; 01_day indicates the second day of the forecast, while 02_day is the third day of the forecast. Thus, three overlapping periods from different forecast initializations are obtained for every day.

Microphysics, land surface model, cumulus convection and planetary boundary layer (PBL) schemes are the important parameterizations used the WRF-Solar model which greatly impact the accuracy of simulated GHI. The processes of cloud and precipitation formation, including phase changes of water is done through the microphysics scheme [68].

The scheme is crucial for the WRF-Solar configuration as it determines the amount of solar radiation that reaches the surface. The Thompson microphysics scheme is the recommended scheme for the WRF-Solar model. However, since aerosol information in the model improves the accuracy of GHI [62,9,39,31], the Thompson aerosol-aware microphysics scheme [68] was used in this study instead. This scheme accounts for direct feedback between aerosol and cloud microphysics. For the direct effect of aerosol on radiation, we applied the approach of [60] to provide the time-varying AOD_{550} and AE in the model. The aerosol assimilation is not parameterized directly in the model, but rather transferred via the radiative transfer routine in each simulated grid cell where the radiation-aerosol interaction is modeled. The aerosol single scattering albedo (SSA) and aerosol asymmetry parameters are computed based on reference aerosol types and relative humidity [60]. The AOD_{550} and AE from CAMS were used for the fully coupled aerosol-cloud-radiation feedback in the WRF-Solar model and updated 3-hourly. The data from CAMS have also been used in previous studies for GHI forecasting [67]. The use of direct aerosol in the WRF-Solar model is realized with the RRTMG scheme for shortwave radiation as well as the scheme for longwave radiation [27].

The exchange of energy, water, and momentum between the atmosphere and the Earth's surface is parametrized in the land surface model [19]. In this study, we used the Noah land surface model, a commonly used choice in WRF-Solar configurations as it provides a reasonable balance between computational efficiency and precision[54]. The Yonsei University PBL scheme was chosen, as it effectively captures the processes affecting solar radiation at the surface [56]. Cumulus schemes play a crucial role in climate models as they present a physically based representation of cloud processes. However, there are some limitations in the sub-grid scale clouds representation within cumulus convection schemes, which can be reduced by the use of shallow convection parametrization in the model [12]. Deng's shallow convection parametrization is favored in WRF-Solar to account for feedbacks between the radiation clouds at the sub-grid scale and produce reasonable cloud fractions [12]. The cumulus scheme was deactivated for both domains and replaced with Deng's shallow convection scheme to reduce limitations in sub-grid scale cloud representation. This enables the activation of radiative feedbacks from both shallow and deep cumulus clouds using the mass-flux parameterization integrated into the WRF-Solar model. The max-flux parameterization uses a cloud entraining/detraining model to represent updrafts. In terms of cloud-radiation feedback, the Deng's shallow convection employs two predictive equations for cloud fraction and cloud liquid/ice water content specific to neutrally buoyant clouds, contributing to the radiation scheme[29]. The Fast All-sky Radiation Model (FARMS) was implemented for faster and more accurate predictions of the solar radiation components, as it utilizes a simplified approach instead of complex mathematical algorithms[73]. We used the GHI from the FARMS (SWDOWN2) with gridded output every 1 h. The simulation uses 45 levels of terrain-following eta layers ranging from the surface (1000 hPa) to 50 hPa.

2.4. Methods

2.4.1. Wrf-solar evaluation

The WRF-Solar model produces daily forecasts with hourly time resolution up to 3 days ahead every day for different variables. The analysis is carried out only for the high-resolution domain, i.e., at 3 km. We compared the GHI, the CFC of the model with observational data on 00_day, 01_day and 02_day for all sky conditions. To understand the effect of clouds and aerosols on the forecasted GHI, the evaluation is also carried out under cloudy and clear sky conditions. As in previous studies [62,14], the clearness index (Kt) was used to identify cloudy and clear sky conditions. Different values of Kt are used for cloudy and clear skies, depending on the region considered. Based on prior studies for the region [55,62,63], we defined cloudy sky when $0.12 \leq Kt < 0.35$ and clear sky when $Kt \geq 0.6$. Moreover, the ability of the model during the occurrence of high ADO_{550} at the three sites is assessed using the 90th and 95th percentiles.

Since the evaluation of the GHI forecast is done hourly, we have also selected the corresponding hourly instantaneous value of the different stations. If a value from the AWS is missing in the corresponding hour, then this hourly value is aggregated within the next 30 min for the corresponding hour. If there is still a missing value for the aggregated hourly instantaneous data, it is set as a missing value. These missing hours were excluded from the analysis. Reliable observational data is critical to the accuracy of model performance. A second quality-controlled check of GHI was carried out in accordance with Baseline Surface Radiation Network (BSRN) guidelines. This consists of removing suspect values of the GHI data outside the physically possible limits and extremely rare limits [42]. The analysis only considers GHI measurements taken when the sun's zenith angle (SZA) is less than 75° to eliminate errors caused by measurement uncertainties at sunrise and sunset and their seasonal variations [21].

2.4.2. Error metrics

Error metrics provide an objective evaluation of the model's accuracy. They are quantitative measures of the error between the forecasted and observed GHI. For this study, we used the root-mean-square error (RMSE, Eq. (2) and the mean absolute error (MAE, Eq. (3). We also calculated the normalized RMSE (nRMSE, Eq. (4) and normalized MAE (nMAE, Eq. (5). Moreover, the Pearson's correlation (R, Eq. (6), the index of agreement (IOA, Eq. (7) and the mean bias error (MBE, Eq. (8) are also used for the model evaluation.

$$RMSE = \sqrt{\sum_{i=1}^{n} \frac{(P_i - O_i)^2}{n}} \tag{2}$$

$$MAE = \frac{1}{n}\sum_{i=1}^{n}(|P_i - O_i|) \tag{3}$$

$$nRMSE = \left[\frac{RMSE}{max(O) - min(O)}\right] * 100 \tag{4}$$

$$nMAE = \left[\frac{MBE}{max(O) - min(O)}\right] * 100 \tag{5}$$

$$R = \frac{\sum_{i=1}^{n}(O_i - \underline{O})(P_i - \underline{P})}{\sqrt{\sum_{i=1}^{n}(O_i - \underline{O})^2 \sum_{i=1}^{n}(P_i - \underline{P})^2}} \tag{6}$$

$$IOA = 1 - \frac{\sum_{i=1}^{n}(P_i - O_i)}{\sum_{i=1}^{n}\left(\left|P_i - \underline{O}\right| \left|O_i - \underline{O}\right|\right)^2} \tag{7}$$

$$MBE = \frac{1}{n}\sum_{i=1}^{n}(P_i - O_i) \tag{8}$$

where P_i is the forecasted value, O_i the observation data at timestep i and n is the number of data points used for comparison. $max(O)$ and $min(O)$ are the maximum and minimum value of the observations.

In addition to these metrics, we incorporated a skill score (s) for the purpose of forecast verification. The skill score (s) serves as a quantification of the relative accuracy of forecasts generated by two forecast systems, with one of them serving as the reference system and it expressed as[50]:

$$s = \frac{A_f - A_r}{A_p - A_r} \tag{9}$$

where A_f, A_p, and A_r indicate are the accuracy of the forecasts of interest, accuracy of the perfect forecasts. s can be based on some statistical metrics, but RMSE is commonly used in solar energy forecasting [76,5,74]. Thus, s is expressed as:

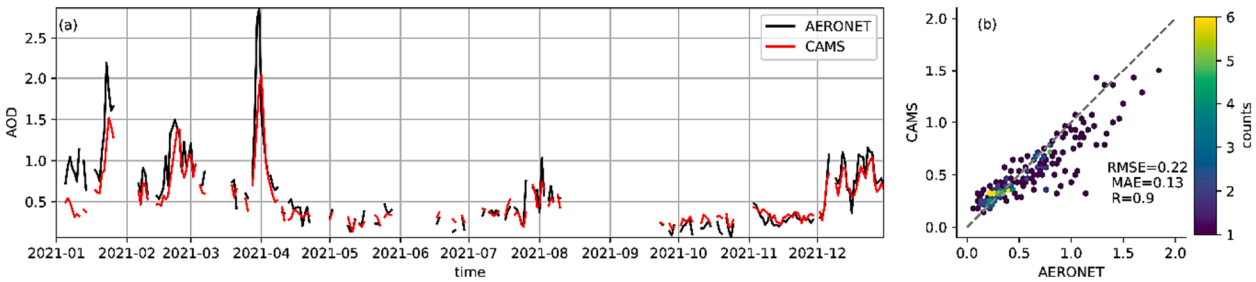

Fig. 4. Comparison of aerosol optical depth at 550 nm (AOD_{550}) between AERONET and the CAMS reanalysis datasets for 2021 at Koforidua. Panel (a) shows the time series, while panel (b) shows the scatter plot between the two datasets. RMSE, MAE and R are the root mean square error, mean absolute error and Pearson correlation, respectively.

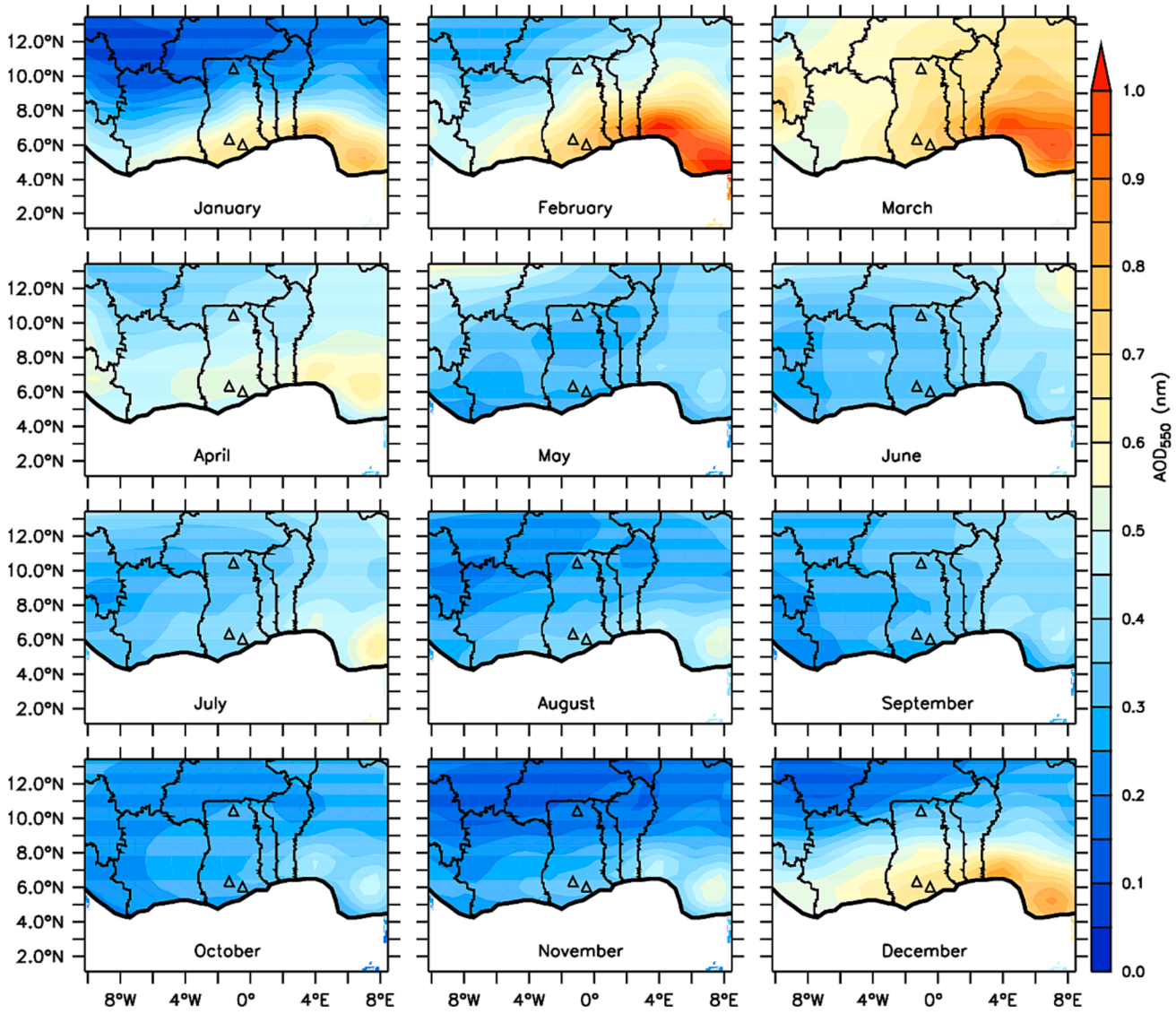

Fig. 5. Spatial distribution of monthly averaged aerosol optical depth at 550 (AOD_{550}) from CAMS reanalysis data for the year 2021. The triangle indicates the different automatic weather stations.

$$s = 1 - \frac{RMSE(f,x)}{RMSE(r,x)} \tag{10}$$

where f, r, and x denote forecasts of interest, reference forecasts, and observations, respectively. When $s > 0$, it means that the forecast is better than the reference forecast, while and $s < 0$ indicates that the forecast performs worse than the reference forecast. A value of $s = 0$ implies that the forecast's performance is equivalent to that of a reference forecast.

The reference forecasts can be produced by either persistence or climatology methods. However, both approaches can be also combined to have an optimum reference forecast; this method is strongly

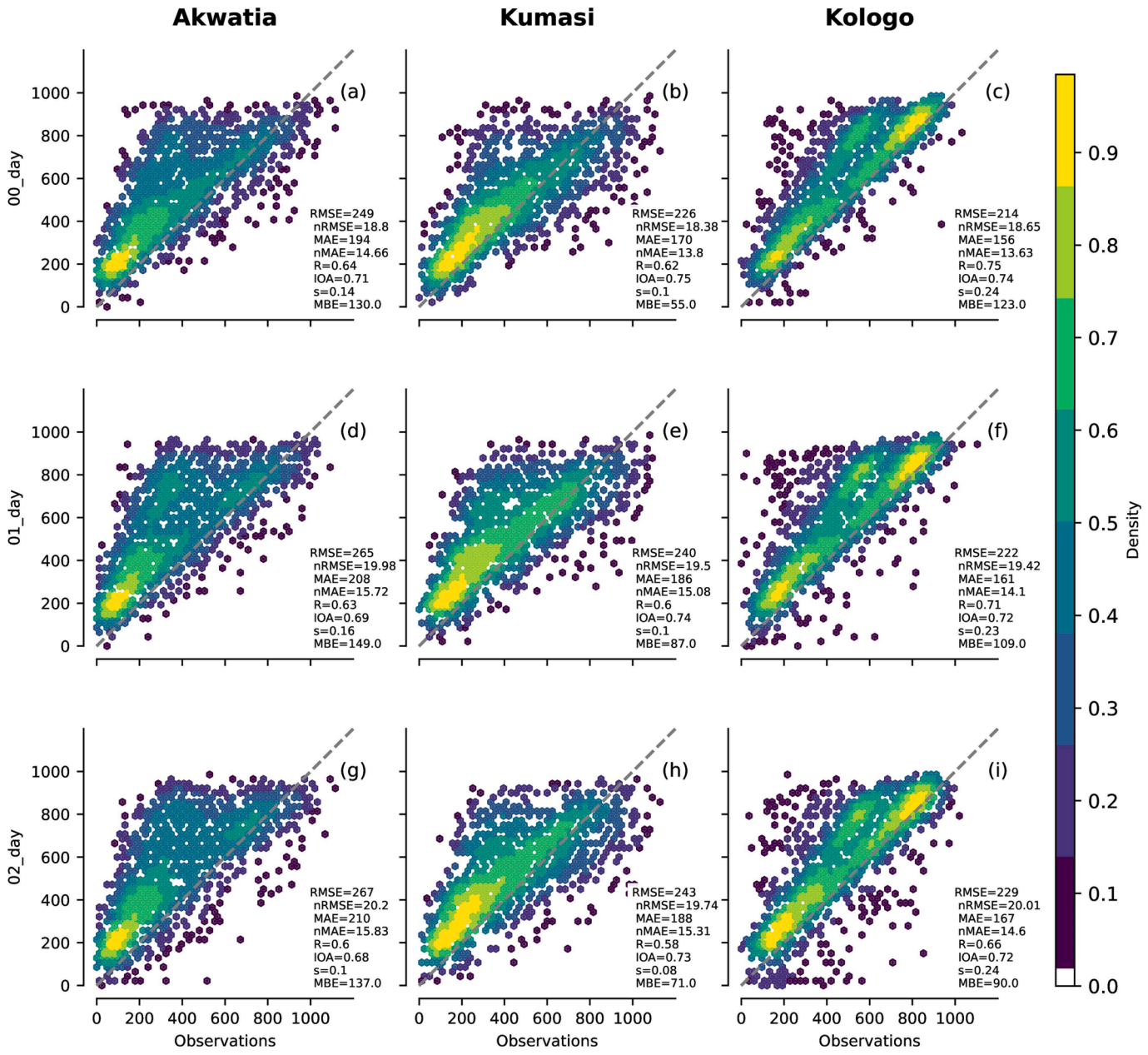

Fig. 6. All-sky evaluation of WRF-Solar simulations of hourly forecasted GHI density versus observational data for weather stations using a normalized Gaussian kernel function with values between 0 and 1 for the year 2021. The rows depict the forecast lead time, with "00_day" representing the first day, "01_day" the second day, and "02_day" the third day. Each of the column represents a weather station with its respective name given on the top. RMSE, R, IOA, MAE, s, and MBE are root-mean-square error, Pearson correlation, index of agreement, and mean absolute error, skill score and the mean bias error, respectively. The terms nRMSE and nMAE indicate the normalized RMSE and MAE, respectively.

recommended by [76] in solar energy applications. Therefore, we used the optimal convex combination of climatology and persistence methods to produce the reference forecast. A single valued internal reference forecast of each of the three stations for the year 2021 when SZA $< 75^{\circ}$ is used for the climatology method. As for the persistence approach, 48-hour-ahead predictions were used. For more details on the optimal convex combination of climatology and persistence methods, please see Yang [74].

3. Results and discussions

3.1. Comparisons between CAMS and AERONET AOD_{550}

Fig. 4 shows the daily time series and scatter plot of CAMS and AERONET data from AOD_{550} for the year 2021 at the Koforidua station. The AERONET system provides AOD information at inconsistent times that are automatically identified as moments of clear sky conditions [61]. Consequently, there are substantial and inherent gaps in the data. These gaps were excluded from the CAMS data for the assessment. In general, CAMS can mimic the seasonal pattern of AERONET. CAMS is able to capture the lower values of AOD_{550} that occur mainly during the rainy season. Both data agree on the two maxima of AOD during the dry season (January and April). An underestimation of CAMS is observed in the peak values of AOD_{550} with a deviation of 0.8 in January and 1 in April. The biases observed in CAMS could be related to persistent clouds in the region that hinder proper aerosol retrievals due to the lack of clear sky conditions [20]. However, both data sets have a high correlation value of about ~ 0.9, an RMSE $= 0.22$ and MAE $= 0.13$. A good annual

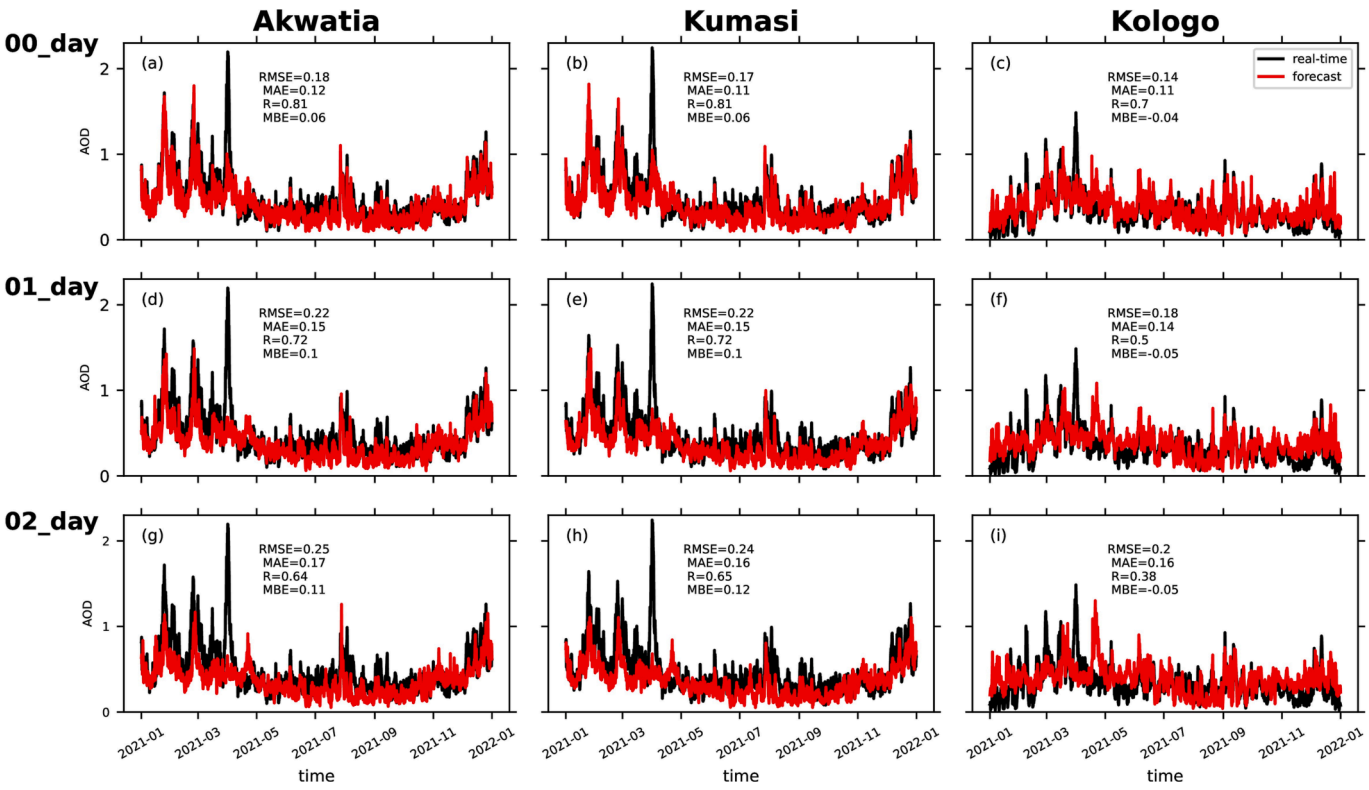

Fig. 7. Comparison of 3-hour time series of the forecasted from WRF-Solar model and real-time aerosol optical depth at 550 nm (AOD_{550}) for the year 2021. The real-time data, represented by the black line, was obtained from the CAMS real-time measurement, while the forecasted AOD_{550} is represented by the red line from the WRF-Solar model. The days are labeled as "00_day" for the first day, "01_day" for the second day, and "02_day" for the third day of the forecast. (For interpretation of the references to colour in this figure legend, the reader is referred to the web version of this article.)

correlation of AOD has been shown for the period 2016–2020 with CAMS reanalysis data[48], like the findings of Léon et al. (2021) when comparing AERONET AOD550 with MODIS data at Koforidua. In summary, CAMS is able to reproduce the pattern of the observation and also to slightly peak the magnitude at lower values of AOD_{550}.However, CAMS reanalyse underestimates high AOD_{550} values occurring in the dry season.

3.1.1. *Characterizations of aerosol*

Fig. 5 illustrates the spatial distribution of AOD_{550} over the study area on a monthly basis using CAMS reanalysis data. The spatial distribution of AOD_{550} shows the month-to-month variability. December to March indicate a high aerosol load, especially in the southern region (Akwatia and Kumasi). April reveals moderately elevated AOD_{550} values compared to the subsequent months, with an average value of 0.4–0.6. The AOD_{550} in this part is mainly due to biomass burning [20]. According to Mari et al. [44], this biomass burning results from vegetation fires transported from Central Africa. In addition, mineral dust aerosols from the Sahara desert and anthropogenic pollutants contribute to the high AOD levels in the area[13]. This combination of different aerosol types leads to a complex atmospheric interaction in the region, which could affect the performance of the model during high AOD. The northern part of Ghana (Kologo) experiences considerable AOD loads during these months but less than the southern part. The average AOD_{550} value ranges between 0.2 and 0.8, with March showing the highest value. Mineral dust aerosols from Saharan dust aloft are the main source of AOD in the area [53].

3.2. *WRF-solar evaluation*

3.2.1. *All-sky*

The GHI forecast for the 3 days ahead for the year 2021 under all sky conditions of the different AWS is shown in Fig. 6. In general, WRF-Solar performs better at all stations and lead time than the reference data as shown by the values of s. Most of the s values are comparable to the forecast days of different stations. However, WRF-Solar performance of the GHI forecast increases towards the north for all 3 days ahead. Kologo shows the highest performance compared to Kumasi and Akwatia. Thus, on the first day of the forecast, Kologo has RMSE of 214 $W.m^{-2}$, MAE of 156 $W.m^{-2}$ with s value of 0.24, while Kumasi (RMSE = 226 $W.m^{-2}$, MAE = 170 $W.m^{-2}$, s = 0.1) and Akwatia (RMSE = 249 $W.m^{-2}$, MAE = 194 $W.m^{-2}$, s = 0.14) show low performance. Nevertheless, at all three sites the model shows an overestimation of the GHI forecast for the 3 days ahead with the largest bias at Akwatia (MBE = 130, 149, and 137 $W.m^{-2}$ for 00_day, 01_day and 02_day, respectively). Overall, the WRF-Solar model performs better in forecasting GHI in cloud-free regions than in cloudy regions. This holds true when analyzing satellite or reanalysis data estimated in GHI [63,64]). Moreover, the performance of the model decreases as the duration of the forecast day increases.

WRF-Solar's performance is better on the first day than on the second and third days. For example, in Akwatia, the 00_day shows a value of RMSE = 249 $W.m^{-2}$ (18.8 %), MAE = 194 $W.m^{-2}$ (14.66 %), R = 0.64, IOA = 0.71, while on 01_day the model shows a value of RMSE = 265 $W.m^{-2}$ (19.98 %), MAE = 208 $W.m^{-2}$ (15.72 %), R = 0.63, IOA = 0.69, and 02_day has a value of RMSE = 267 $W.m^{-2}$ (20.2 %), MAE = $W.m^{-2}$ 210 (15.83 %), R = 0.6, IOA = 0.68. Additionally, there is not much difference between the GHI predictions for 01_day and 02_day in terms of RMSE compared to 00_day, where there is a difference of about 16 $W.m^{-2}$ between 00_day and 01_day, mainly at the cloudy sites (Akwatia and Kumasi). The deviation is reduced by half at the cloud-free site (Kologo; 8 $W.m^{-2}$). High biases were also found by[37]in the GHI forecast with the WRF model at the Jerez station in Spain under all sky conditions, with 00_day (RMSE = 142 $W.m^{-2}$) performing better than 01_day (RMSE = 147 $W.m^{-2}$) and 02_day (RMSE = 152 $W.m^{-2}$). The

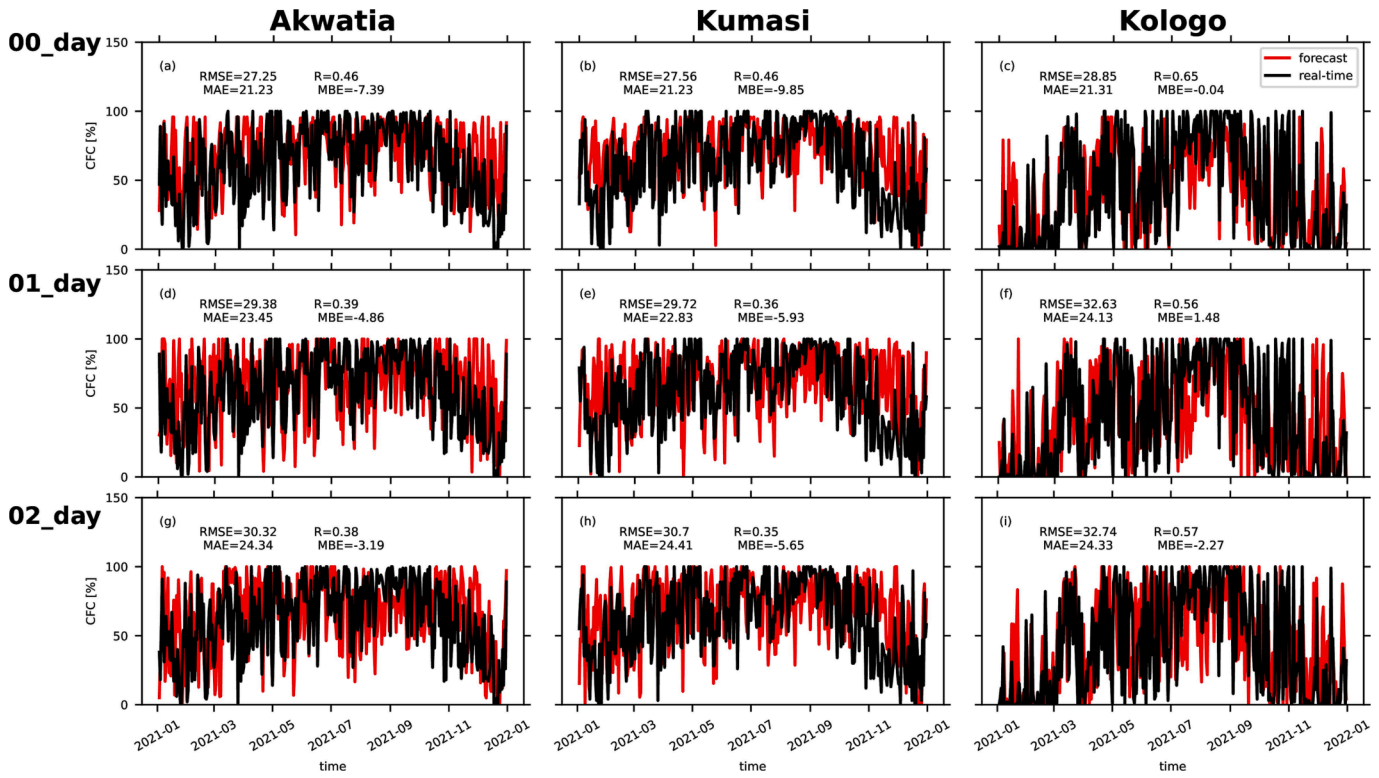

Fig. 8. Similar to Fig. 7 but displays the real-time fractional cloud cover (CFC) from the Interim Climate Data Record (ICDR) SEVIRI (Spinning Enhanced Visible and InfraRed Imager) and the forecasted CFC from the WRF-Solar model.

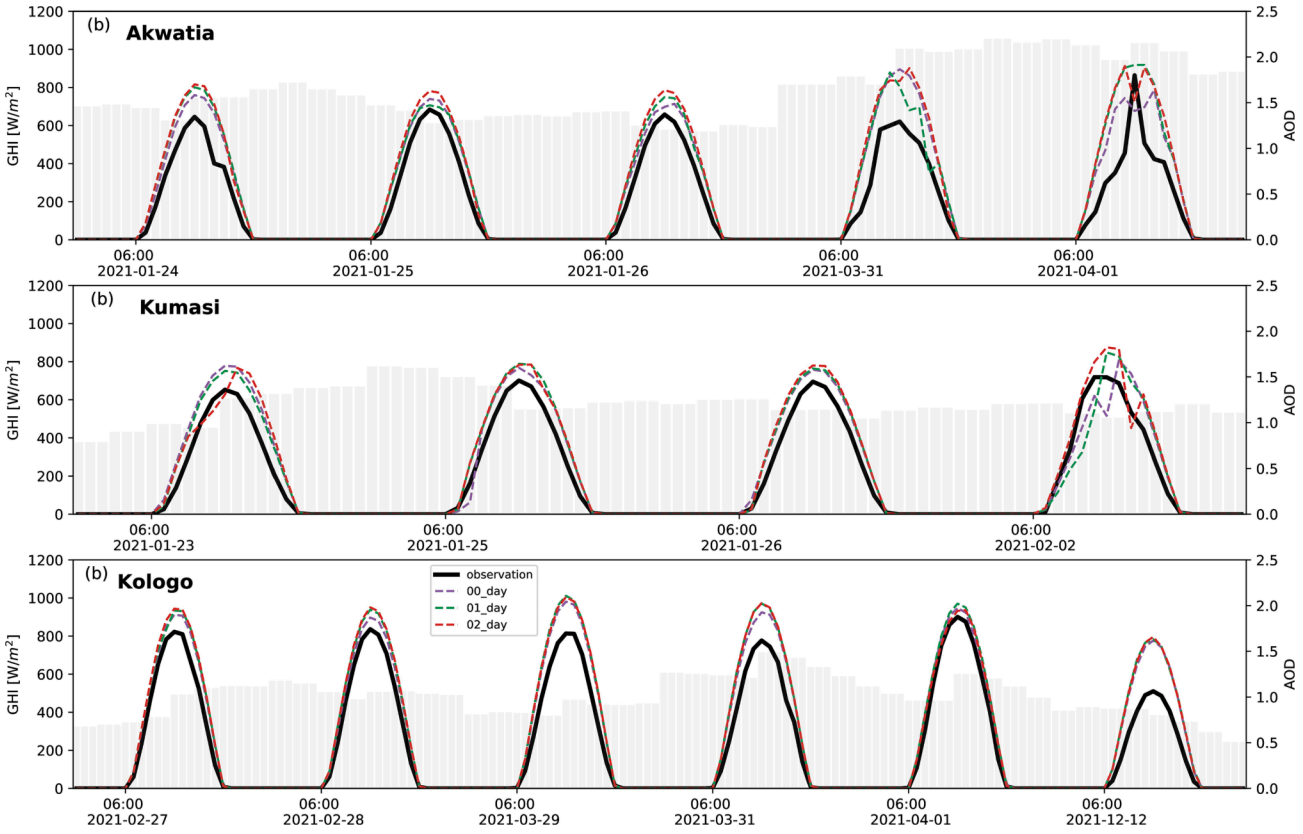

Fig. 9. Diurnal cycle of 3-day ahead forecast in different AWS during a period of high AOD load in the year 2021. Days are identified as "00_day" for the first day, "01_day" for the second day, and "02_day" for the third day of the forecast. The black line indicates the observed GHI, while the purple, green and purple lines show the 00_day, 01_day, and 02_day GHI forecasts, respectively. The gray bar shows the AOD values from CAMS reanalysis. (For interpretation of the references to colour in this figure legend, the reader is referred to the web version of this article.)

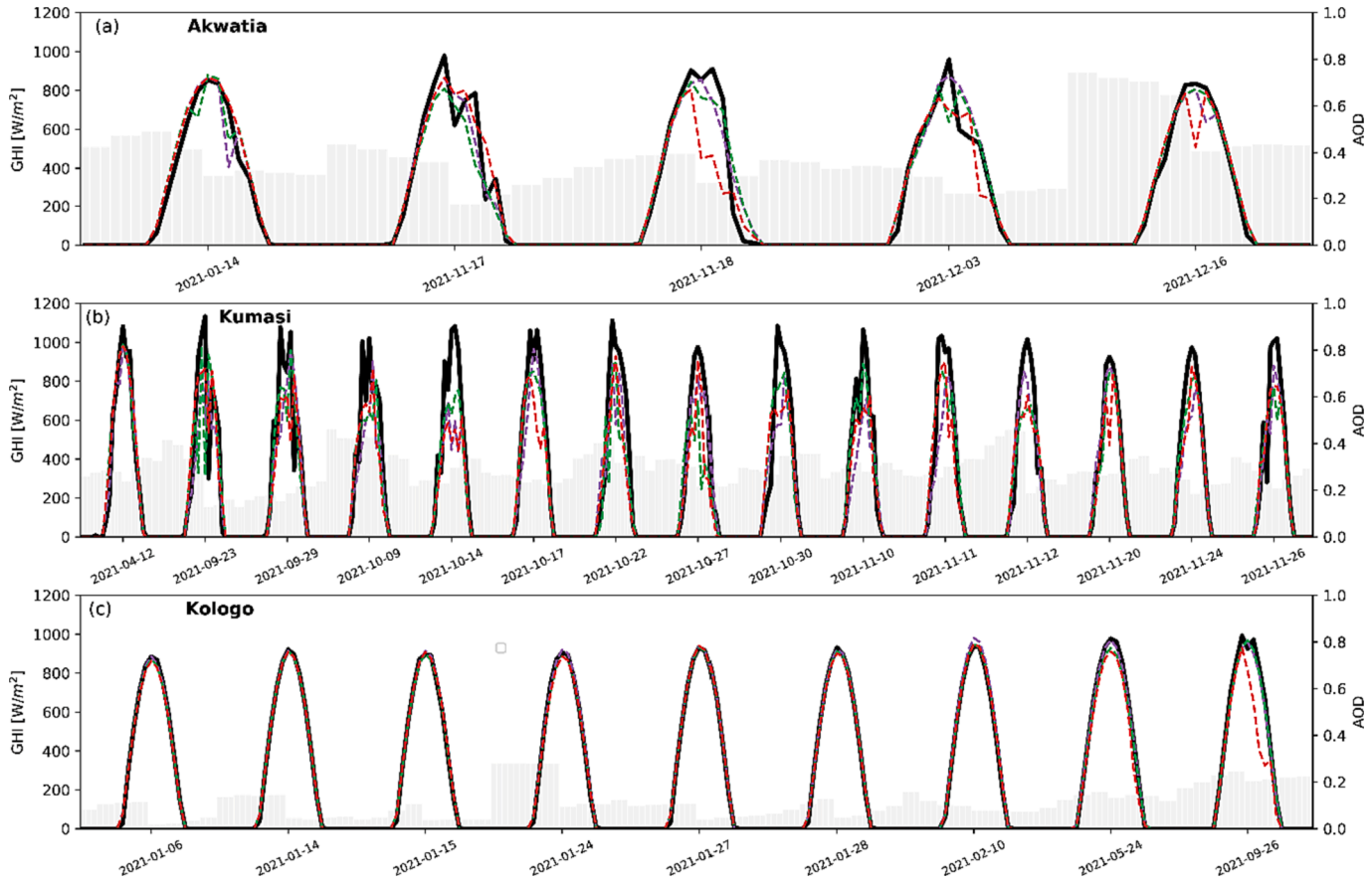

Fig. 10. Similar to Fig. 9, but during clear sky days composites.

discrepancies between the biases of both results could be related to the different climate zones or the model configurations. The high bias in the region could be attributed to the aerosol-radiation or cloud-radiation feedback in the WRF-Solar model. These hypotheses are investigated by showing the forecast AOD_{550} and the CFC.

3.2.2. Predicted aerosol optical depth at 550 nm (AOD_{550})

Fig. 7 shows the 3-day ahead time series of AOD_{550} with real-time data for the year 2021. The figure contains the real-time data from CAMS (3-hourly) and the forecasted AOD_{550} from the WRF-Solar model (averaged over 3 h). The purpose of this analysis is to verify the accuracy of the AOD_{550} forecast vis-à-vis CAMS reanalysis data. The AOD_{550} forecast shows better performance for 00_day compared to 01_day and 02_day. During high AOD_{550} episodes, especially in Akwatia and Kumasi, the prediction fails to capture the magnitude and becomes worse on 01_day and 02_day with a deviation of more than 2. The situation is similar in the case of Kologo, but with a deviation of less than 1. Overall, the AOD_{550} forecast indicates an overestimation for all stations and across all the forecast days. However, the bias of the AOD_{550} forecast is significantly lower for events with low AOD_{550} values. This suggests that the AOD_{550} forecast performs better at low values than at high values. Note that the AOD_{550} from the CAMS data is biased compared to the AERONET data (see section 3.1). Considering all biases, the AOD_{550} forecast from CAMS has a significant bias at high values, especially in the Guinea climate zone (Akwatia and Kumasi). This agrees with the finding by Meilinger and Mekeng [48] who found CAMS to underestimate AOD for high AOD values during the Harmattan period and overestimates AOD for low values during rainy periods when compared to AERONET.

3.2.3. Prediction of fractional cloud cover (CFC)

Another uncertainty in the prediction of GHI could be due to the accuracy of the forecasted CFC in the model. For that, we also plotted the daily averaged time series of real-time CFC from ICDR-SEVIRI and the WRF solar model (Fig. 8). In line with the forecasting performance of AOD_{550} and GHI, the 00_day demonstrates more accurate CFC forecasting compared to the 01_day and 02_day. Across various stations, RMSE and MAE values exhibit consistency for each forecast day, while correlation values show variations. Kologo has the highest correlation value of about 0.65, but this value drops to 0.57 (02_day) and 0.56 (01_day). Akwatia and Kumasi have slightly the same correlation for each forecast day. In general, WRF-Solar tends to overestimate the CFC during the dry season and also during the rainy season at all considered stations and forecast days, but in general, the forecast shows an underestimation. For example, on day_00, the MBE values is 7.39 % for Akwatia, −9.85 % for Kumasi, and −0.04 % for Kologo. Kologo exhibits the least bias, while Kumasi and Akwatia show relatively high bias across all forecast days. The daily CFC of the WRF-Solar model shows biases that could potentially lead to biases in its hourly CFC. The results show that the WRF-Solar model is not able to reproduce reasonable cloud patterns in West Africa, which is prone to low-level clouds [2,10]. This is consistent with the conclusions of Yang et al. [77], who show that the WRF-Solar model leads to inaccuracies in the forecasting of thin and low-level clouds over the CONUS region. This implies the necessity of further improvement of cloud forecasting in the WRF-Solar model to improve the accuracy of GHI forecasting in the region. Nevertheless, there are still uncertainties in the analysis due to the possible bias of the satellite data due to algorithm retrieval issues or missed clouds [6].

3.2.4. Aerosol-radiation interactions in GHI forecasting

Fig. 9 shows the diurnal cycle of forecasted GHI for different AWS on

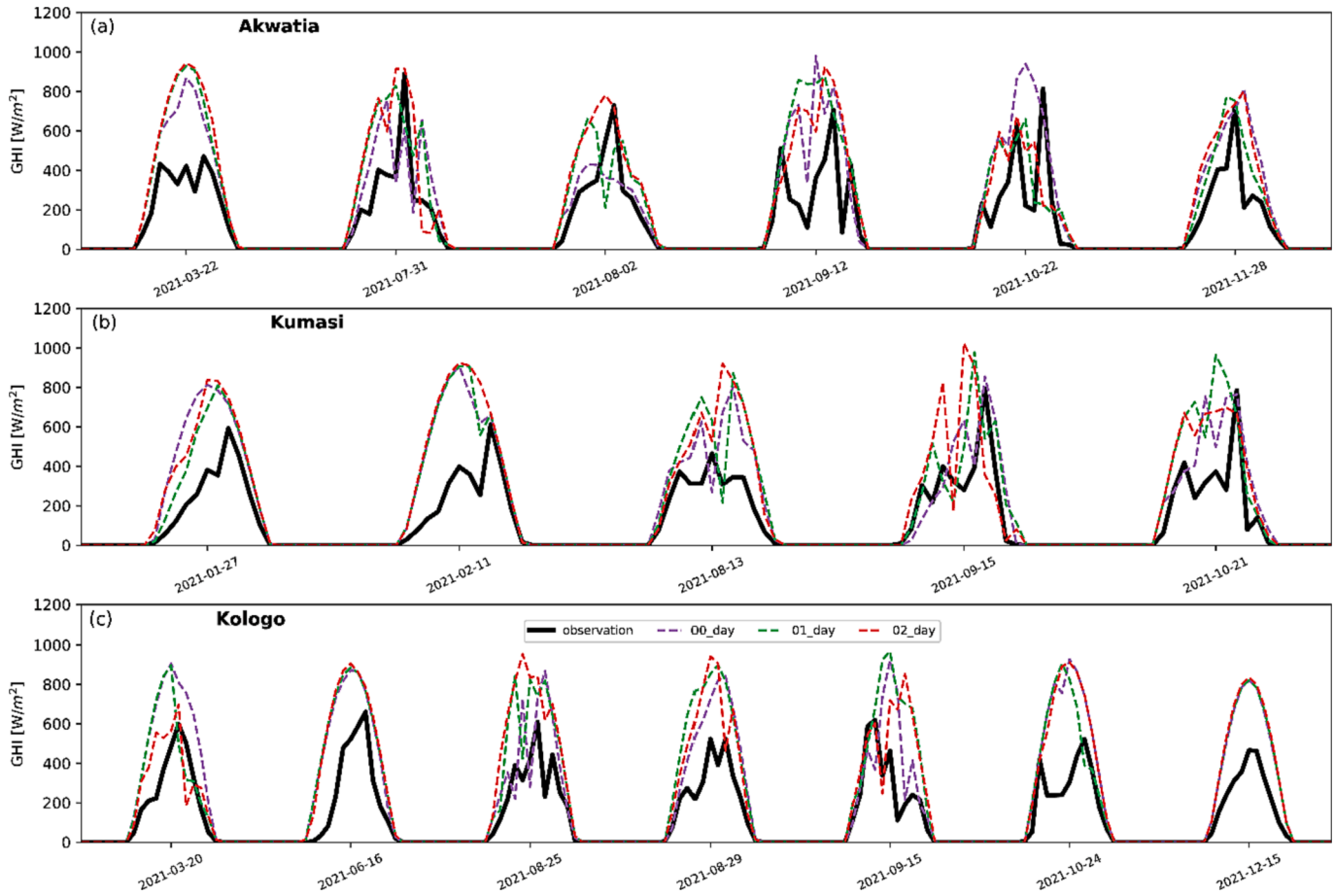

Fig. 11. Similar to Fig. 10, but for cloudy days.

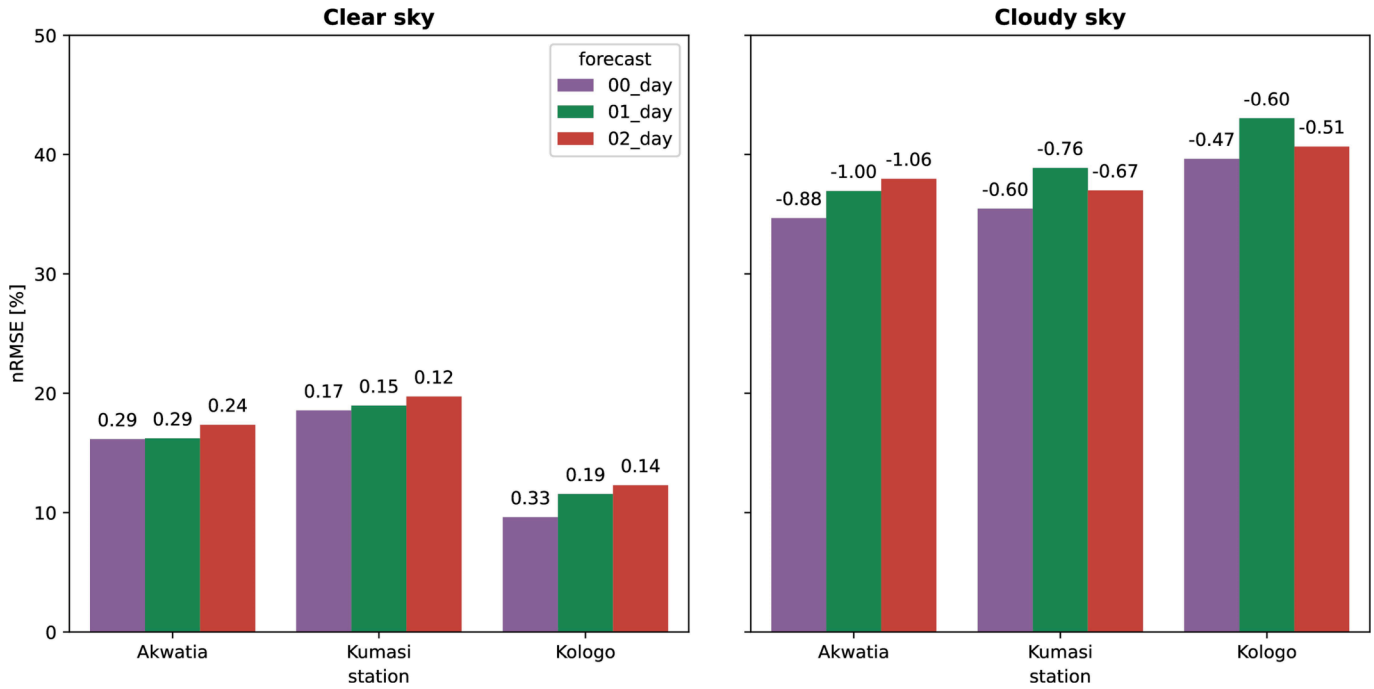

Fig. 12. Bar plot of the normalized root-mean-square-error (nRMSE) of GHI forecasting under clear and cloudy skies for different automatic weather stations (AWS) for the year 2021. The 00_day indicates the first forecast day, while the 01_day and 02_day show the second and the third forecast day, respectively. The value on each barplot indicates the skill score value.

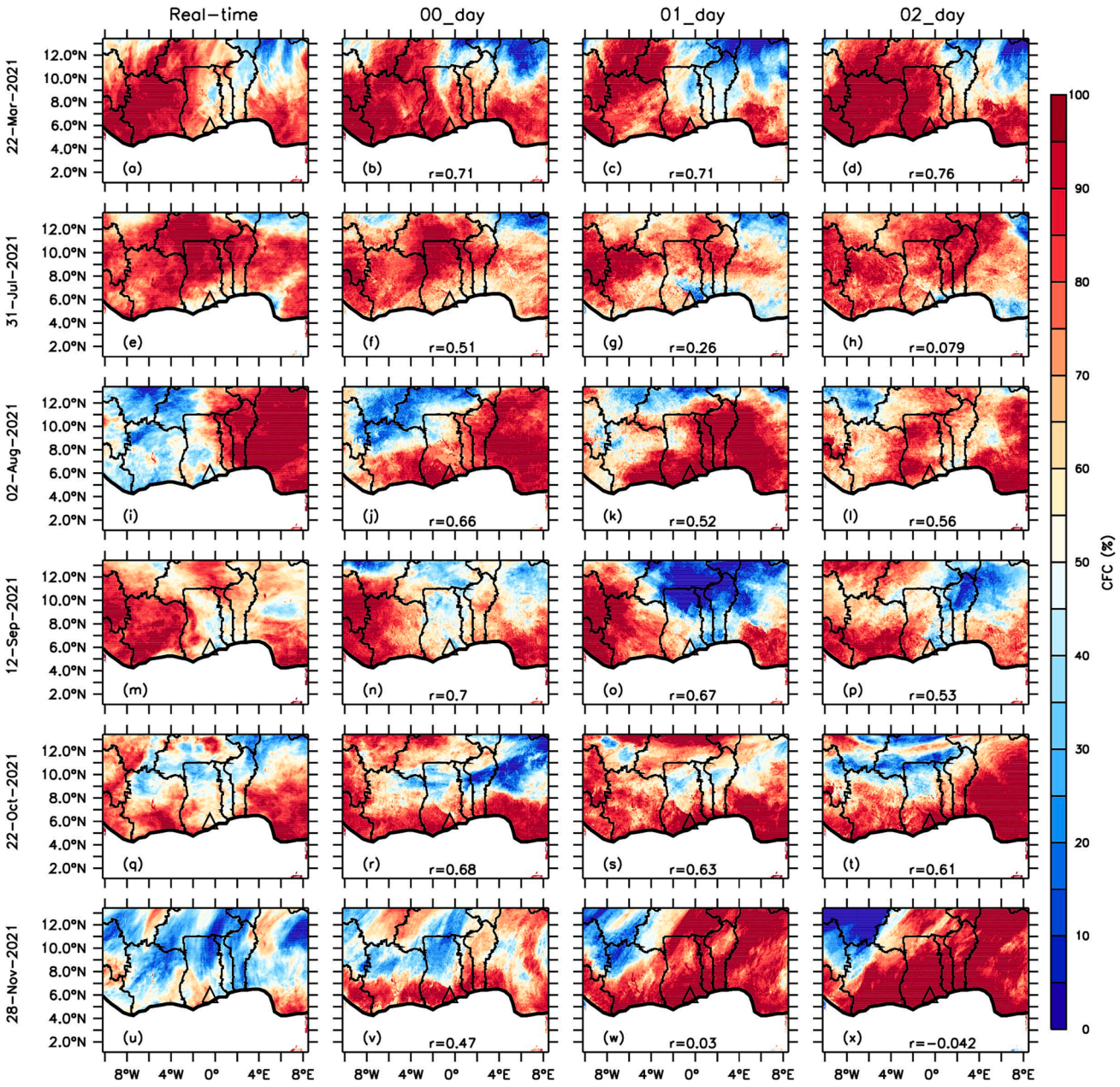

Fig. 13. Spatial distribution of real-time and predicted fractional cloud cover (CFC) for Akwatia on different dates using selected cloudy day composites (displayed on the left side). The real-time data is sourced from the ICDR-SEVIRI dataset, while the predicted data is derived from the WRF-Solar model. The days are labeled as "00_day" for the first day, "01_day" for the second day, and "02_day" for the third day of the forecast. The "r" denotes the spatial correlation between the real-time data and the forecasted data. The triangle represents the location of the automatic weather station.

high AOD days. The figure was generated using the 90th and 95th percentiles of daily AOD data from the CAMS reanalysis for the year 2021 for Akwatia, Kumasi and Kologo, respectively. The dates obtained are consistent with Fig. 5, which shows that the high AOD loading in the region occurs between December and April. In order to reduce the potential impact of clouds during periods of heightened aerosol loading, we have set a threshold of CFC $\leq$ 20 % for the selected dates. The model generally captures the diurnal pattern of GHI during periods of relatively low AOD loading across all stations, with the 00_day forecast performing better than the 01_day and 02_day forecasts. In addition, the WRF-Solar model performs better on some days in Kologo than in Akwatia and Kumasi, likely due to the aerosol types in these areas and/or presence of clouds. The latter is discussed is section 3.2.5. For example, on 1 April 2021, when the maximum AOD exceeded 2 in Akwatia, all forecasted days could not accurately reproduce the pattern of GHI, while the model closely reproduce the pattern of GHI in Kologo, where the maximum of AOD value is below 1.5. However, for relatively low value of AOD (<1.5), the model is able to mimic the pattern of the GHI observation especially in Akwatia and Kumasi where all the forecast days match well the pattern of the observed. Though, the WRF-Solar overestimates the maximum observed GHI in most of days mainly in Kologo. On the other hand, the bias of forecasted AOD during periods of high values could also contribute to the GHI forecasting biases. [22]reports that an existing bias in AOD can lead to a bias in the GH estimate of up to 8 %. The uncertainties in the input AOD or the information loss during AOD data assimilation may lead to adverse indirect effects of aerosol (on cloud and radiative properties) in the model.

3.2.5. *GHI forecasting under clear sky*

Fig. 10 displays the analysis of the direct and/or indirect effects of

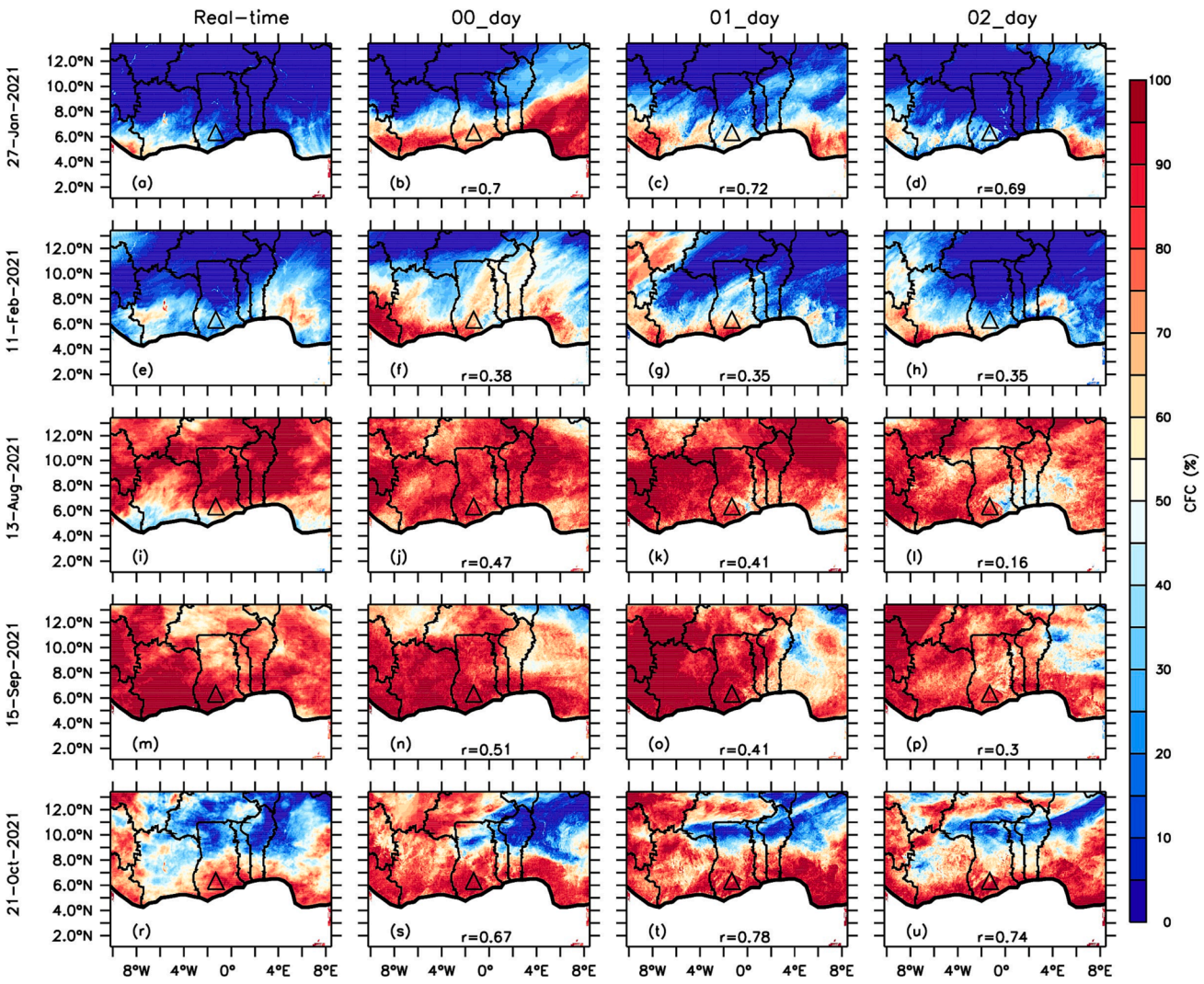

Fig. 14. Similar to Fig. 13, but for Kumasi.

aerosols on radiative properties in GHI forecasting. This shows the diurnal cycle of GHI from the model and observation under clear sky conditions. The figure was constructed using days greater than or equal to the 75th percentile of clear sky days in Akwatia (kt = 0.63) and Kumasi (kt = 0.67) and the 95th percentile in Kologo (kt = 0.75), as the northern region experiences more clear sky days than the southern part (Sawadogo et al., 2022). In Akwatia and Kumasi, certain days exhibit variations in the diurnal pattern of the observed GHI, transitioning from clear to cloudy conditions. These variations are likely due to the frequent occurrence of cloud and/or albedo enhancement effects (Gueymard et al., 2019).

All forecast days (00_day, 01_day and 02_day) are overlaid with the observed GHI on most of the average clear-sky days in Kologo. However, in Akwatia and Kumasi, the 00_day and 01_day agree well with the observed GHI pattern on some day. The results indicate that the model is able to reproduce the observed GHI pattern in the northern region where mineral dust is predominant, but not in the southern region where biomass burning, mineral dust and anthropogenic aerosol coexist. This poor performance could be attributed to the bias in the forecasting of AOD from CAMS data (see Fig. 6). This is consistent with previous studies that have shown that the deterioration of the WRF-Solar model performance in forecasting GHI under clear skies is due to a large bias in AOD input, rather than radiation parameterization [29,60]. Another reason could be due to the different radiation schemes used in WRF-Solar (RRTMG) and CAMS (ecRad) or to the partial loss of multispectral aerosol information resulting from the sole use of the CAMS AOD_{550} field in the WRF-Solar model [39].

3.2.6. *GHI forecasting under cloudy sky*

To generate the selected days in the composite of cloudy days, we determined the 90th percentile of the total cloudy days for different AWS. The WRF-Solar model overestimated GHI under cloudy conditions for all stations (Fig. 11) and could not replicate the observational pattern. The 00_day GHI forecast had the least bias, indicating that uncertainties in GHI forecasting during cloudy conditions exist in the region. This is consistent with previous studies[40]; [64]) highlighting that the WRF-Solar model produces uncertainties in GHI forecasting during cloudy days. These limitations may be due to the cloud-radiation feedback associated with cloud transmittance.

However, using Kt to identify cloudy days could lead to misidentification of cloudy days due to aerosols or pollution. Therefore, we examined the spatial distribution of CFC and AOD_{550} for the different days in Fig. 11 for each station (see Appendix) using the reference data (ICDR-SEVIRI and CAMS) and the WRF-Solar forecasting. This helped us to isolate true cloudy days and also to investigate the feedback between clouds, aerosols and radiation in relation to GHI forecasting in the region.

For instance, on 12 September 2021, the daily mean AOD_{550} at Akwatia was less than 0.3 (see Appendix Fig. 16 m), while the CFC based on real-time data was above 70 % (see Appendix Fig. 12 m), which we

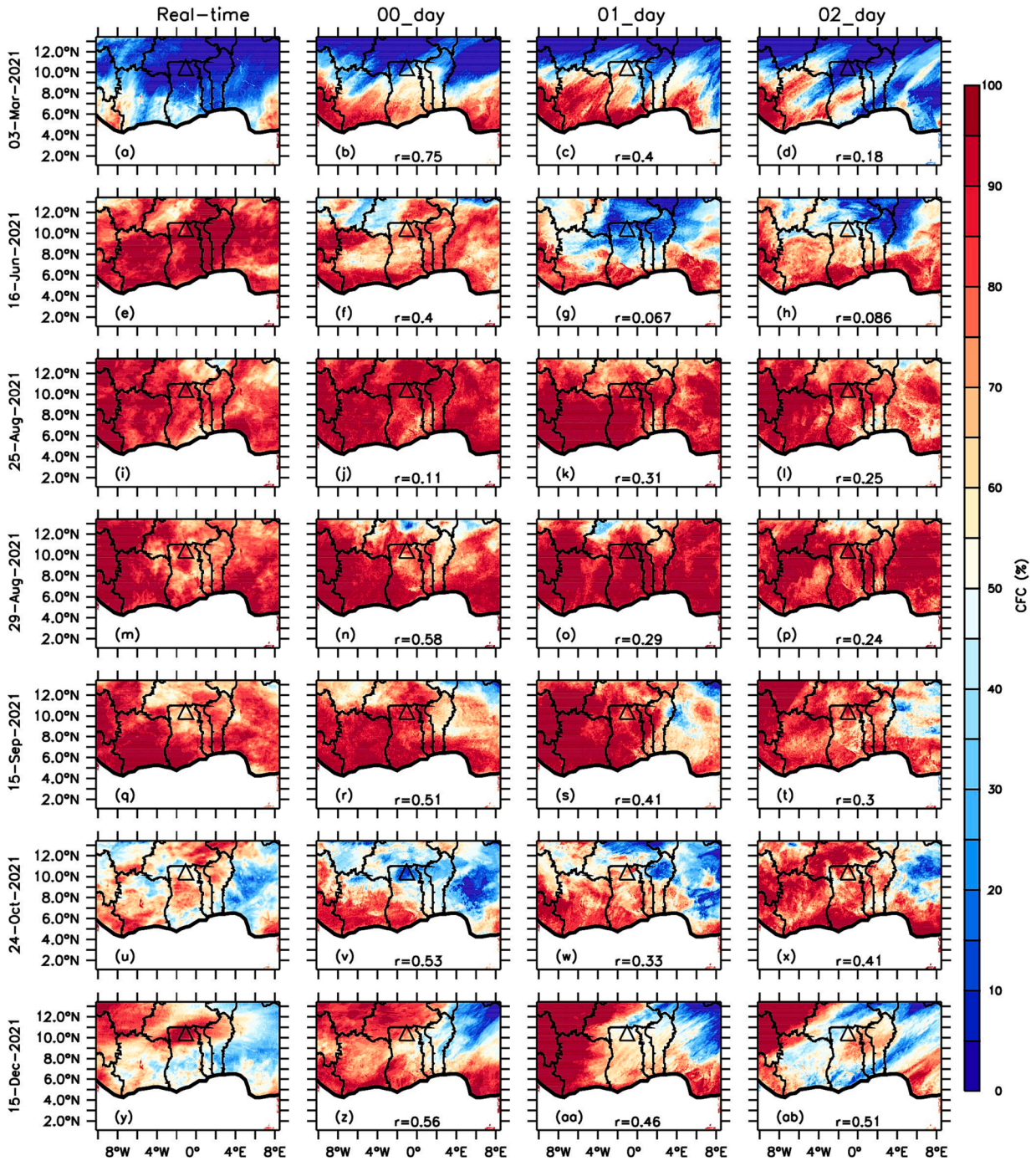

Fig. 15. Similar to Fig. 13, but for Kologo.

classified as a cloudy day. Similar classified cloudy days were observed in Kumasi (15 September 2021; see Appendix Fig. 14 m & Fig. 17 m) and Kologo (25 August 2021; see Appendix Fig. 15 i & Fig. 18 i). The WRF-Solar model was able to predict the CFC in all stations for days ahead, albeit with some notable biases. However, the uncertainty in the GHI prediction under cloudy conditions suggests that the model is not able to simulate the rapid change in cloud fluctuation in the area at the right time (Fig. 11 a). This shows that the forecast of cloud properties remains a major challenge for the WRF-Solar model, which may also contribute to the uncertainties in the GHI forecast [30,32] in the region due to the frequent occurrence of low-level stratus clouds during the rainy season.

On 22 March 2021 at Akwatia (see Appendix Fig. 13 a & Fig. 16 a) and on 16 June 2021 at Kologo (see Appendix Fig. 15 e & Fig. 18 e), there was a relatively high AOD load and CFC, and the model could not replicate the observational pattern (Fig. 11). The pattern of all predictions for days ahead was similar to that of clear sky days. These "pseudo clear sky" conditions, produced by the model, could be related to the dissipation of clouds. Indeed, while aerosols can act as cloud condensation nuclei (CCN), increasing high concentrations of aerosols in non-precipitating clouds can lead to smaller cloud droplets that evaporate faster, which may result in clear skies under dry conditions[17]. This suggests that the WRF-Solar model tends to produce clear skies instead of cloudy skies when high AOD interacts with clouds in the region. This also indicates uncertainties in the predictive ability of the WRF-Solar model when it comes to high AOD values resulting from biomass burning, anthropogenic pollution and dust interacting with

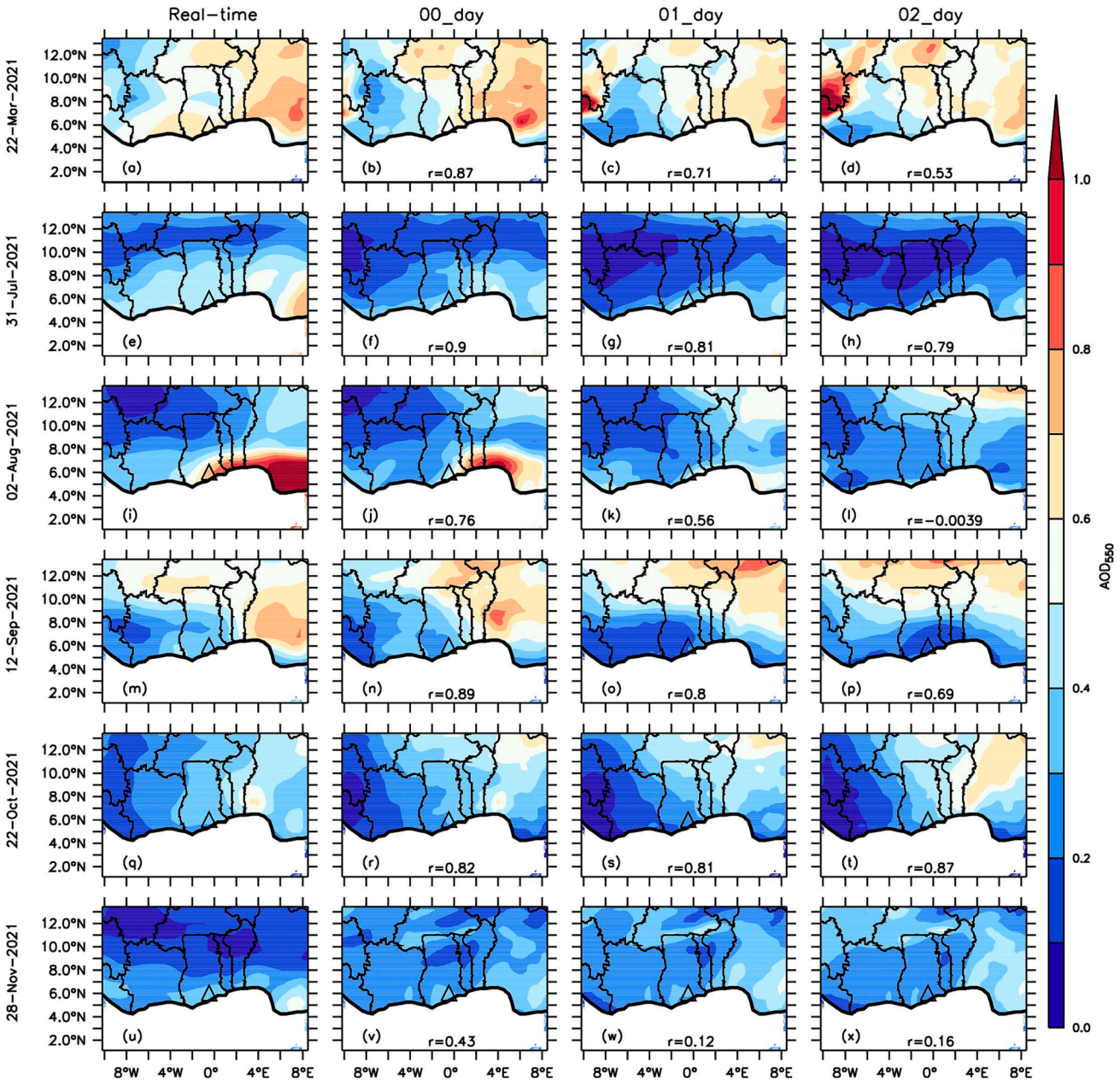

Fig. 16. Spatial distribution of real-time and predicted AOD_{550} for Akwatia on different dates using selected cloudy day composites (displayed on the left side The real-time data comes from the CAMS data, while the predicted data is derived from the WRF-Solar model. The days are labeled as "00_day" for the first day, "01_day" for the second day, and "02_day" for the third day of the forecast. The "r" denotes the spatial correlation between the real-time data and the forecasted data. The triangle represents the location of the automatic weather station.

clouds in the region. This could be due to the assimilation process of the AOD in the aerosol-aware Thompson-Eidhammer microphysics scheme [40] and/or the feedback between cloud, aerosol and radiation, as the AOD is directly transferred into the radiative transfer routine[60]. Nevertheless, the pattern of the WRF-Solar is much better than that of Akwatia on that date. This is line with Liu et al. [40] , where they found that the performance of the WRF-Solar model depends of the type of aerosols and sources.

Overall, the study concludes that the aerosol-cloud-radiation feedback in the WRF-Solar model can lead to uncertainties in the prediction of GHI on cloudy sky days when high AOD values are involved, which is consistent with previous findings[40]. The bias in AOD and CFC forecasts may contribute to these large uncertainties.

3.2.7. *GHI forecasting under clear and cloudy skies*

Fig. 12 illustrates nRMSE and s of GHI forecasting for clear and cloudy days using different AWS when SZA $> 75^{\circ}$. In clear skies, the 3-day ahead forecast of GHI in Kologo outperforms the 00_day forecast in Akwatia and Kumasi. This is also shown by the values of s where the value of s is about 0.33 in Kologo and 0.17 and 0.29 in Kumasi and Akwatia, respectively. The relative low skill score values found could be explained by the employed method (optimal convex combination of climatology and persistence) used. Typically, this method yields lower skill scores compared to solely relying on climatology or persistence approach [47,75]. Liu et al. [41] demonstrated a shortfall ranging from 0.2 to 0.6 in the skill score for solar irradiance forecasting across the CONUS region when employing the optimal convex combination of climatology and persistence method. They also suggested that using this method provides opportunities for improving solar irradiance

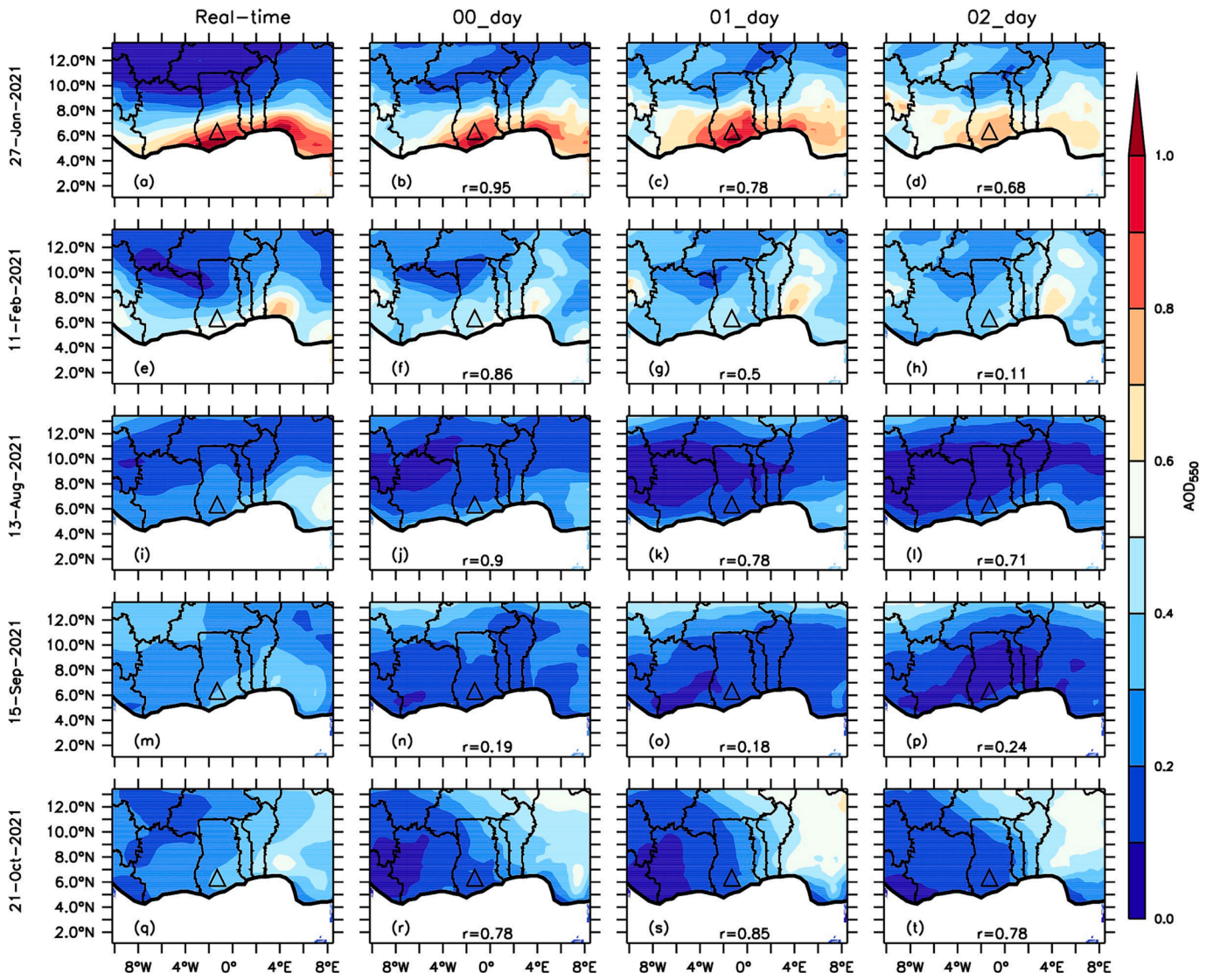

Fig. 17. Similar to Fig. 16, but for Kumasi.

forecasting. However, among the forecasts in Kologo, the 00_day forecast has the best performance (9.62 %), followed by the 01_day (11.56 %) and 02_day (12.29 %) forecasts. The performance difference between the 02_day forecast in Kologo and the 00_day forecast in Akwatia and Kumasi is approximately 3.86 % and 6.27 %, respectively. The discrepancy between Kologo and the other two sites could be due to variations in aerosol types and sources or uncertainties associated with the input AOD in the WRF-Solar model. In Akwatia and Kumasi, the 00_day and 01_day forecasts are similar, indicating that the 00_day and 01_day forecast are preferable in Akwatia and Kumasi, while in Kologo the 3-day ahead GHI forecast could be used.

Under cloudy day composites, WRF-Solar performs worse in all the stations and forecast days with s ranges from −1.06 to −0.47. This suggests that the reference forecast perform better than the real forecast. However, the 00_day forecast is preferred in all AWS under cloudy skies. The poor performance of Kologo under cloudy skies could be related to the fact that the model does not properly represent the occurrence of cumulus clouds, as cumulus clouds are common in this area during the rainy season. This was also evident in the CONUS domain, where the deviation of the frequency of cumulus clouds from the WRF-Solar model could reach about 45 % [77]. Overall, Kologo shows the best performance under all-sky conditions. This suggests that the model compensates for the large bias in cloudy skies with clear skies.

The uncertainties in GHI forecasting under cloudy skies may be also related to cloud predictions in the WRF-Solar model and the indirect effect of aerosols on clouds in the region. Clouds are difficult to predict due to their complex dynamics and microphysics. To improve GHI forecasting under cloudy skies,[30,32] suggested initializing clouds in the WRF-Solar model using satellite observations to detect and advect clouds within the model domain, providing more realistic cloud fields. Another method to reduce uncertainties in GHI forecasting could be the use of ensemble probabilistic systems (EPS) to generate multiple cloud scenarios based on perturbations of initial boundary conditions [77] or model parameterizations. Those two approaches could substantially reduce uncertainties in GHI forecasting and provide more accurate values. Accuracy in GHI forecasting will help various solar energy applications, such as plant installation, demand and supply balancing, load dispatch scheduling, storage management, trading of generated power in the market [35].

4. Summary and conclusion

The study has investigated the capability of the WRF-Solar model for GHI forecasting in the West African region, especially Ghana. The model's accuracy is compared with three reliable AWS: Akwatia, Kumasi and Kologo for 2021. The ECMWF-HRES forecast data provided the

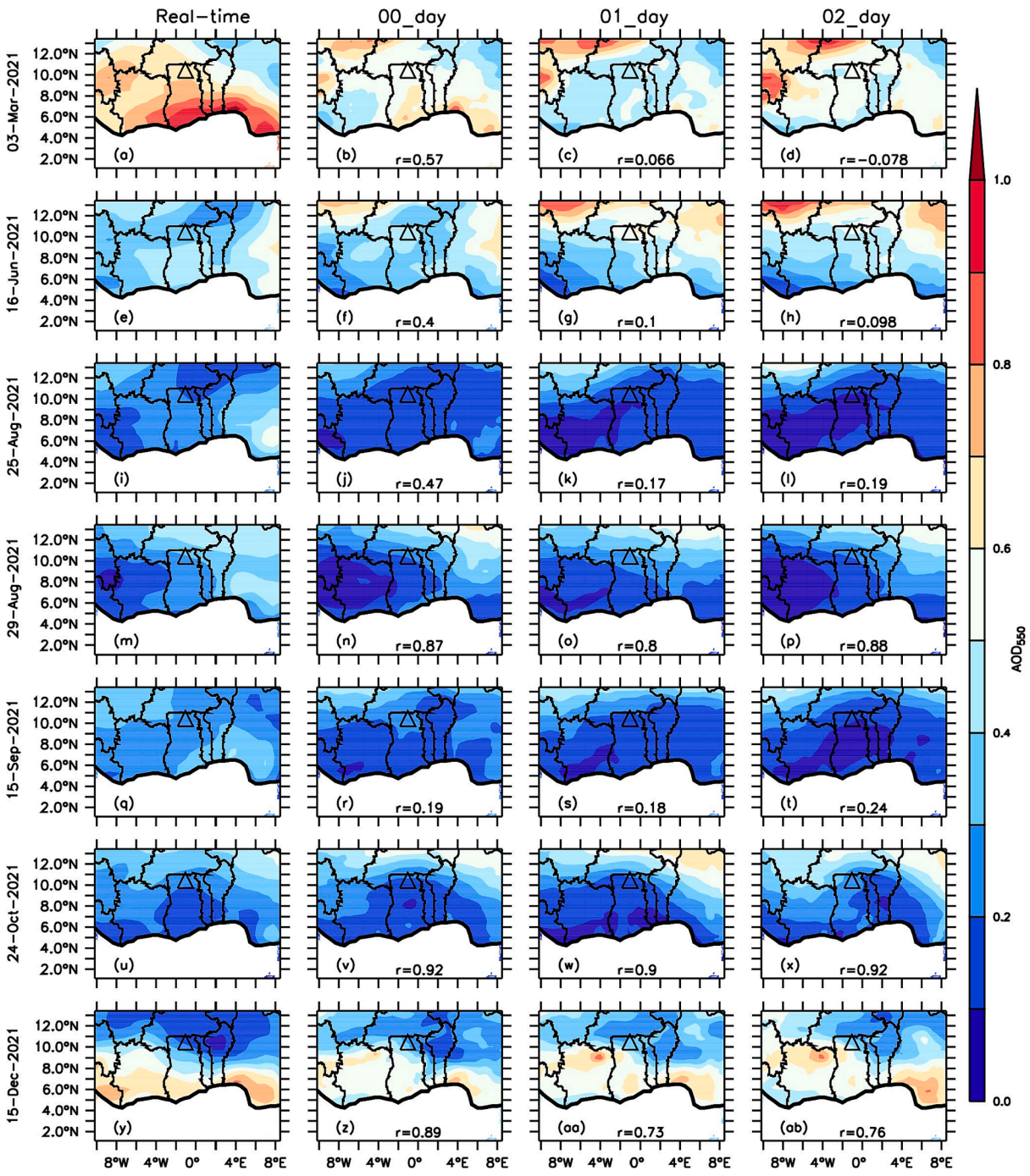

Fig. 18. Similar to Fig. 16, but for Kologo.

initial and lateral boundary conditions. Moreover, we fully coupled the WRF-Solar model with AOD from CAMS datasets. We analyzed the model under various weather conditions: cloudy, clear, and all-sky at an instantaneous hourly rate. We also investigated the aerosol-cloud-radiation feedback on a specific day. The results of this study can be summarized as follows:

- CAMS AOD_{550} shows a considerable negative bias compared to AERONET data in the southern part of Ghana during the dry period and a positive bias during the rainy season.
- CAMS AOD_{550} predicts high values poorly and its prediction accuracy decreases with longer forecast days.
- For all-sky conditions, GHI forecasting performs best for 00_day lead time and at the Kologo AWS.
- There are some notable biases in the CFC predictions from the WRF-Solar model.
- WRF-Solar model is able to reproduce the observed GHI diurnal cycle under high AOD conditions in most of the selected days.
- For clear skies, GHI forecasting performs better for 00_day, 01_day and 02_day at Kologo, and for 00_day and 01_day at Akwatia and Kumasi.
- Under cloudy skies, the WRF-Solar model exhibits large uncertainties at all the AWS and 00_day GHI forecast should be used.

In this study, the WRF-Solar model has shown the capability of

forecasting GHI in the West African region mainly under clear-sky conditions. However, on cloudy days, the model has larger uncertainties. The results of our study align with previous ones using the WRF-Solar model but differ in terms of uncertainties [23,31,37]. This could be related to the frequent low-level clouds in the region, as the WRF-Solar model cannot predict them accurately[77]. Moreover, the substantial uncertainties in GHI forecasting could be attributed to uncertainties in the input AOD during data assimilation within the model. The aerosol-cloud-radiation feedback parametrization should be improved when the high AOD is ingested in the model. One potential study is to compare AOD data from the CAMS and NASA's GEOS-5 global models, while using the fully coupled WRF-Solar model for GHI forecasting in the region. Additionally, studies should explore the use of the Multi-sensor Advection Diffusion nowCast (MAD-WRF) model in combination with the WRF-Solar model to initialize clouds using satellite data on cloud and relative humidity. Furthermore, it would be useful to assess the performance of the WRF-Solar EPS model in conjunction with the WRF-Solar model, as this can provide valuable insights into the uncertainties associated with GHI forecasting in the region.

Our study found that the WRF-Solar model accurately forecast GHI up to 3 days in advance under clear-sky conditions. We identified some limitations in the analyzing of GHI forecasting. Specifically, using a clearness index for cloud classification may result in false cloudy days due to aerosol loading or pollution and also not a really clear sky day mainly in cloudy regions. In contrast, using a cloud mask may accurately classify cloudy and clear sky days. Additionally, our comparison of simulated CFC with observational data on a daily basis did not allow for deeper analysis. Despite these limitations, our study provides insight into the use of the WRF-Solar model for GHI forecasting in West Africa, which can benefit solar energy managers in energy management, planning, grid integration, and cost reduction efforts. The results of our study may also be useful for healthcare centers seeking to enhance their PV-based energy solutions in Ghana.

Funding

This research is part of the project EnerSHelF, funded by the German Federal Ministry of Education and Research (BMBF) as part of the CLIENT II program. Funding reference number: 03SF0567D. It is additionally co-funded by the WASCAL CONCERT project grant number: 01LG2089A, BMBF) as part of the WASCAL research programme.

CRediT authorship contribution statement

Windmanagda Sawadogo: Conceptualization, Methodology, Software, Figures, Formal analysis. **Benjamin Fersch:** Writing – review & editing, Conceptualization, Methodology. **Jan Bliefernicht:** Writing – review & editing, Conceptualization, Methodology. **Stefanie Meilinger:** Writing – review & editing. **Thomas Rummler:** Writing – review & editing. **Seyni Salack:** Writing – review & editing. **Samuel Guug:** Writing – review & editing. **Harald Kunstmann:** Supervision. All authors have read and agreed to the published version of the manuscript.

Declaration of Competing Interest

The authors declare that they have no known competing financial interests or personal relationships that could have appeared to influence the work reported in this paper.

Acknowledgment

We express our gratitude to the administration and technical staff of Saint Dominic Hospital in Akwatia, Saint Michael Hospital in Kumasi, and the Kologo Health Center in the Upper East Region for allowing us to install and operate our weather stations on their premises, and for their support during the installation and maintenance of the weather stations. The authors thank the Copernicus Atmosphere Monitoring Service (CAMS) datasets for providing the aerosol data. We are also grateful to the European Centre for Medium-range Weather Forecast (ECMWF) for enabling access to the operational forecast data. We also thank the Satellite Application Facility on Climate Monitoring for providing the fractional cloud cover data from Interim Climate Data Record (ICDR) of SEVIRI (Spinning Enhanced Visible and InfraRed Imager).

Appendix A

References

[1] J. Antonanzas, N. Osorio, R. Escobar, R. Urraca, F.J. Martinez-de-Pison, F. Antonanzas-Torres, Review of photovoltaic power forecasting, Sol. Energy 136 (2016) 78–111, https://doi.org/10.1016/j.solener.2016.06.069.

[2] J.N.A. Aryee, L.K. Amekudzi, E.I. Yamba, Low-Level Cloud Development and Diurnal Cycle in Southern West Africa During the DACCIWA Field Campaign: Case Study of Kumasi Supersite, Ghana, J. Geophys. Res. Atmos. 126 (11) (2021), https://doi.org/10.1029/2020JD034028.

[3] N. Benas, S. Finkensieper, M. Stengel, G.-J. van Zadelhoff, T. Hanschmann, R. Hollmann, J.F. Meirink, The MSG-SEVIRI-based cloud property data record CLAAS-2, Earth Syst. Sci. Data 9 (2) (2017) 415–434, https://doi.org/10.5194/essd-9-415-2017.

[4] E. Bessah, W. Amponsah, S.O. Ansah, A. Afrifa, B. Yahaya, C.S. Wemegah, M. Tanu, L.K. Amekudzi, W.A. Agyare, Climatic zoning of Ghana using selected meteorological variables for the period 1976–2018, Meteorol. Appl. 29 (1) (2022), https://doi.org/10.1002/met.2049.

[5] R. Blaga, A. Sabadus, N. Stefu, C. Dughir, M. Paulescu, V. Badescu, A current perspective on the accuracy of incoming solar energy forecasting, Prog. Energy Combust. Sci. 70 (2019) 119–144, https://doi.org/10.1016/j.pecs.2018.10.003.

[6] C. Bulgin, C. Merchant, D. Ghent, L. Klüser, T. Popp, C. Poulsen, L. Sogacheva, Quantifying Uncertainty in Satellite-Retrieved Land Surface Temperature from Cloud Detection Errors, Remote Sens. (Basel) 10 (4) (2018) 616, https://doi.org/10.3390/rs10040616.

[7] S. Chaaraoui, M. Bebber, S. Meilinger, S. Rummeny, T. Schneiders, W. Sawadogo, H. Kunstmann, Day-Ahead Electric Load Forecast for a Ghanaian Health Facility Using Different Algorithms, Energies 14 (2) (2021) 409, https://doi.org/10.3390/en14020409.

[8] E. Chandiwana, C. Sigauke, A. Bere, Twenty-Four-Hour Ahead Probabilistic Global Horizontal Irradiance Forecasting Using Gaussian Process Regression, Algorithms 14 (6) (2021) 177, https://doi.org/10.3390/a14060177.

[9] X. Cheng, D. Ye, Y. Shen, D. Li, J. Feng, Studies on the improvement of modelled solar radiation and the attenuation effect of aerosol using the WRF-Solar model with satellite-based AOD data over north China, Renew. Energy 196 (2022) 358–365.

[10] D.K. Danso, S. Anquetin, A. Diedhiou, K. Kouadio, A.T. Kobea, Daytime low-level clouds in West Africa—Occurrence, associated drivers, and shortwave radiation attenuation, Earth Syst. Dyn. 11 (4) (2020) 1133–1152.

[11] J.M.S. de Araujo, Performance comparison of solar radiation forecasting between WRF and LSTM in Gifu, Japan, Environ. Res. Commun. 2 (4) (2020) 045002, https://doi.org/10.1088/2515-7620/ab7366.

[12] Deng, A., Gaudet, B., Dudhia, J., & Alapaty, K. (2014). *Implementation and Evaluation of a New Shallow Convection Scheme in WRF*.

[13] A. Deroubaix, L. Menut, C. Flamant, J. Brito, C. Denjean, V. Dreiling, A. Fink, C. Jambert, N. Kalthoff, P. Knippertz, R. Ladkin, S. Mailler, M. Maranan, F. Pacifico, B. Piguet, G. Siour, S. Turquety, Diurnal cycle of coastal anthropogenic pollutant transport over southern West Africa during the DACCIWA campaign, Atmos. Chem. Phys. 19 (1) (2019) 473–497, https://doi.org/10.5194/acp-19-473-2019.

[14] Y. Du, H. Shi, J. Zhang, X. Xia, Z. Yao, D. Fu, B. Hu, C. Huang, Evaluation of MERRA-2 hourly surface solar radiation across China, Sol. Energy 234 (2022) 103–110, https://doi.org/10.1016/j.solener.2022.01.066.

[15] ECMWF. (2023). *CAMS: Global atmospheric composition forecast data documentation*. https://confluence.ecmwf.int/display/CKB/CAMS%3A+Global+atmospheric+composition+forecast+data+documentation.

[16] Edwards, P. N. (2013). Predicting the Weather: An Information Commons for Europe and the World. *Cosmopolitan Commons: Sharing Resources and Risks Across Borders*, 155–184.

[17] J. Fan, Y. Wang, D. Rosenfeld, X. Liu, Review of Aerosol-Cloud Interactions: Mechanisms, Significance, and Challenges, J. Atmos. Sci. 73 (11) (2016) 4221–4252, https://doi.org/10.1175/JAS-D-16-0037.1.

[18] Finkensieper, S., Stengel, M., Selbach, N., Rainer, H., Werscheck, M., & Meirink, J. F. (2018). *ICDR SEVIRI Clouds—Based on CLAAS-2 Methods, Satellite Application Facility on Climate Monitoring*.

[19] R.A. Fisher, C.D. Koven, Perspectives on the Future of Land Surface Models and the Challenges of Representing Complex Terrestrial Systems, J. Adv. Model. Earth Syst. 12 (4) (2020), https://doi.org/10.1029/2018MS001453.

[20] C. Flamant, P. Knippertz, A.H. Fink, A. Akpo, B. Brooks, C.J. Chiu, H. Coe, S. Danuor, M. Evans, O. Jegede, N. Kalthoff, A. Konaré, C. Liousse, F. Lohou, C. Mari, H. Schlager, A. Schwarzenboeck, B. Adler, L. Amekudzi, V. Yoboué, The

Dynamics–Aerosol–Chemistry–Cloud Interactions in West Africa Field Campaign: Overview and Research Highlights, Bull. Am. Meteorol. Soc. 99 (1) (2018) 83–104, https://doi.org/10.1175/BAMS-D-16-0256.1.
[21] J. Flemming, V. Huijnen, J. Arteta, P. Bechtold, A. Beljaars, A.-M. Blechschmidt, M. Diamantakis, R.J. Engelen, A. Gaudel, A. Inness, et al., Tropospheric chemistry in the Integrated Forecasting System of ECMWF, Geosci. Model Dev. 8 (4) (2015) 975–1003.
[22] C.A. Gueymard, Uncertainties in Modeled Direct Irradiance Around the Sahara as Affected by Aerosols: Are Current Datasets of Bankable Quality? J. Sol. Energy Eng. 133 (3) (2011) https://doi.org/10.1115/1.4004386.
[23] Gueymard, C., & Jimenez, P. (2019). *Validation of Real-Time Solar Irradiance Simulations Over Kuwait Using WRF-Solar*. 10.18086/eurosun2018.09.14.
[24] S. Gyamfi, M. Modjinou, S. Djordjevic, Improving electricity supply security in Ghana—The potential of renewable energy, Renew. Sustain. Energy Rev. 43 (2015) 1035–1045, https://doi.org/10.1016/j.rser.2014.11.102.
[25] T. Haiden, M. Janousek, F. Vitart, Z.B. Bouallègue, L. Ferranti, F. Prates, D. Richardson, Evaluation of ECMWF forecasts, including the 2018 upgrade, European Centre for Medium Range Weather Forecasts Reading, UK, 2018.
[26] B.N. Holben, T.F. Eck, I. Slutsker, D. Tanré, J.P. Buis, A. Setzer, E. Vermote, J. A. Reagan, Y.J. Kaufman, T. Nakajima, F. Lavenu, I. Jankowiak, A. Smirnov, AERONET—A Federated Instrument Network and Data Archive for Aerosol Characterization, Remote Sens. Environ. 66 (1) (1998) 1–16, https://doi.org/10.1016/S0034-4257(98)00031-5.
[27] M.J. Iacono, J.S. Delamere, E.J. Mlawer, M.W. Shephard, S.A. Clough, W. D. Collins, Radiative forcing by long-lived greenhouse gases: Calculations with the AER radiative transfer models, J. Geophys. Res. Atmos. 113 (D13) (2008).
[28] A. Inness, M. Ades, A. Agusti-Panareda, J. Barré, A. Benedictow, A.-M. Blechschmidt, J.J. Dominguez, R. Engelen, H. Eskes, J. Flemming, et al., The CAMS reanalysis of atmospheric composition, Atmos. Chem. Phys. 19 (6) (2019) 3515–3556.
[29] P.A. Jiménez, S. Alessandrini, S.E. Haupt, A. Deng, B. Kosovic, J.A. Lee, L. Delle Monache, The role of unresolved clouds on short-range global horizontal irradiance predictability, Mon. Weather Rev. 144 (9) (2016) 3099–3107.
[30] P.A. Jiménez, J. Dudhia, G. Thompson, J.A. Lee, T. Brummet, Improving the cloud initialization in WRF-Solar with enhanced short-range forecasting functionality: The MAD-WRF model, Sol. Energy 239 (2022) 221–233, https://doi.org/10.1016/j.solener.2022.04.055.
[31] P.A. Jimenez, J.P. Hacker, J. Dudhia, S.E. Haupt, J.A. Ruiz-Arias, C.A. Gueymard, G. Thompson, T. Eidhammer, A. Deng, WRF-SOLAR: Description and clear-sky assessment of an augmented NWP model for solar power prediction, Bull. Am. Meteorol. Soc. (2016), https://doi.org/10.1175/BAMS-D-14-00279.1.
[32] P.A. Jiménez, J. Yang, J.-H. Kim, M. Sengupta, J. Dudhia, Assessing the WRF-Solar model performance using satellite-derived irradiance from the National Solar Radiation Database, J. Appl. Meteorol. Climatol. 61 (2) (2022) 129–142.
[33] T. Kåberger, Progress of renewable electricity replacing fossil fuels, Global Energy Interconnection 1 (1) (2018) 48–52, https://doi.org/10.14171/J.2096-5117.GEI.2018.01.006.
[34] P. Knippertz, A.H. Fink, R. Schuster, J. Trentmann, J.M. Schrage, C. Yorke, Ultra-low clouds over the southern West African monsoon region, Geophys. Res. Lett. 38 (21) (2011).
[35] P. Kumari, D. Toshniwal, Deep learning models for solar irradiance forecasting: A comprehensive review, J. Clean. Prod. 318 (2021) 128566, https://doi.org/10.1016/j.jclepro.2021.128566.
[36] C.S. Lai, C. Zhong, K. Pan, W.W.Y. Ng, L.L. Lai, A deep learning based hybrid method for hourly solar radiation forecasting, Expert Syst. Appl. 177 (2021) 114941, https://doi.org/10.1016/j.eswa.2021.114941.
[37] V. Lara-Fanego, J.A. Ruiz-Arias, D. Pozo-Vázquez, F.J. Santos-Alamillos, J. Tovar-Pescador, Evaluation of the WRF model solar irradiance forecasts in Andalusia (southern Spain), Sol. Energy 86 (8) (2012) 2200–2217.
[38] J.A. Lee, S.E. Haupt, P.A. Jiménez, M.A. Rogers, S.D. Miller, T.C. McCandless, Solar irradiance nowcasting case studies near Sacramento, J. Appl. Meteorol. Climatol. 56 (1) (2017) 85–108.
[39] J.A. Lee, P.A. Jiménez, J. Dudhia, Y.-M. Saint-Drenan, Impacts of the Aerosol Representation in WRF-Solar Clear-Sky Irradiance Forecasts over CONUS, J. Appl. Meteorol. Climatol. (2022), https://doi.org/10.1175/JAMC-D-22-0059.1.
[40] Y. Liu, Y. Qian, S. Feng, L.K. Berg, T.W. Juliano, P.A. Jiménez, Y. Liu, Sensitivity of solar irradiance to model parameters in cloud and aerosol treatments of WRF-solar, Sol. Energy 233 (2022) 446–460, https://doi.org/10.1016/j.solener.2022.01.061.
[41] B. Liu, D. Yang, M.J. Mayer, C.F. Coimbra, J. Kleissl, M. Kay, Y. Shen, Predictability and forecast skill of solar irradiance over the contiguous United States, Renew. Sustain. Energy Rev. 182 (2023) 113359.
[42] Long, C. N., & Dutton, E. G. (2010). *BSRN Global Network recommended QC tests, V2. X*.
[43] F.M. Lopes, H.G. Silva, R. Salgado, A. Cavaco, P. Canhoto, M. Collares-Pereira, Short-term forecasts of GHI and DNI for solar energy systems operation: Assessment of the ECMWF integrated forecasting system in southern Portugal, Sol. Energy 170 (2018) 14–30, https://doi.org/10.1016/j.solener.2018.05.039.
[44] C.H. Mari, G. Cailley, L. Corre, M. Saunois, J.L. Attié, V. Thouret, A. Stohl, Tracing biomass burning plumes from the Southern Hemisphere during the AMMA 2006 wet season experiment, Atmos. Chem. Phys. 8 (14) (2008) 3951–3961, https://doi.org/10.5194/acp-8-3951-2008.
[45] V. Masson-Delmotte, P. Zhai, H.-O. Pörtner, D. Roberts, J. Skea, P.R. Shukla, A. Pirani, W. Moufouma-Okia, C. Péan, R. Pidcock, et al., Global warming of 1.5 C, An IPCC Special Report on the Impacts of Global Warming of 1 (5) (2018) 43–50.
[46] P. Mathiesen, J. Kleissl, Evaluation of numerical weather prediction for intra-day solar forecasting in the continental United States, Sol. Energy 85 (5) (2011) 967–977, https://doi.org/10.1016/j.solener.2011.02.013.
[47] M.J. Mayer, D. Yang, Calibration of deterministic NWP forecasts and its impact on verification, Int. J. Forecast. 39 (2) (2023) 981–991.
[48] S. Meilinger, A.Z. Mekeng, Influence of aerosols on photovoltaic power in Ghana: Case study from Koforidua, Copernicus Meetings, 2022.
[49] P. Mpfumali, C. Sigauke, A. Bere, S. Mulaudzi, Day ahead hourly global horizontal irradiance forecasting—Application to South African data, Energies 12 (18) (2019) 3569.
[50] A.H. Murphy, Skill Scores Based on the Mean Square Error and Their Relationships to the Correlation Coefficient, Mon. Weather Rev. 116 (12) (1988) 2417–2424, https://doi.org/10.1175/1520-0493(1988)116<2417:SSBOTM>2.0.CO;2.
[51] T. Mutavhatsindi, C. Sigauke, R. Mbuvha, Forecasting hourly global horizontal solar irradiance in South Africa using machine learning models, IEEE Access 8 (2020) 198872–198885.
[52] I. Neher, S. Crewell, S. Meilinger, U. Pfeifroth, J. Trentmann, Photovoltaic power potential in West Africa using long-term satellite data, Atmos. Chem. Phys. 20 (21) (2020) 12871–12888, https://doi.org/10.5194/acp-20-12871-2020.
[53] S.E. Nicholson, Climate of the Sahel and West Africa, in: Oxford Research Encyclopedia of Climate Science, Oxford University Press, 2018, https://doi.org/10.1093/acrefore/9780190228620.013.510.
[54] G.-Y. Niu, Z.-L. Yang, K.E. Mitchell, F. Chen, M.B. Ek, M. Barlage, A. Kumar, K. Manning, D. Niyogi, E. Rosero, M. Tewari, Y. Xia, The community Noah land surface model with multiparameterization options (Noah-MP): 1. Model description and evaluation with local-scale measurements, J. Geophys. Res. 116 (D12) (2011) D12109, https://doi.org/10.1029/2010JD015139.
[55] E.C. Okogbue, J.A. Adedokun, B. Holmgren, Hourly and daily clearness index and diffuse fraction at a tropical station, Ile-Ife, Nigeria, Int. J. Climatol. 29 (8) (2009) 1035–1047.
[56] Olson, J. B., Kenyon, J. S., Angevine, W., Brown, J. M., Pagowski, M., Sušelj, K., & others. (2019). *A description of the MYNN-EDMF scheme and the coupling to other components in WRF–ARW*.
[57] R. Perez, S. Kivalov, J. Schlemmer, K. Hemker, D. Renné, T.E. Hoff, Validation of short and medium term operational solar radiation forecasts in the US, Sol. Energy 84 (12) (2010) 2161–2172, https://doi.org/10.1016/j.solener.2010.08.014.
[58] R. Perez, E. Lorenz, S. Pelland, M. Beauharnois, G. Van Knowe, K. Hemker, D. Heinemann, J. Remund, S.C. Müller, W. Traunmüller, G. Steinmauer, D. Pozo, J. A. Ruiz-Arias, V. Lara-Fanego, L. Ramirez-Santigosa, M. Gaston-Romero, L. M. Pomares, Comparison of numerical weather prediction solar irradiance forecasts in the US, Canada and Europe, Sol. Energy 94 (2013) 305–326, https://doi.org/10.1016/j.solener.2013.05.005.
[59] M. Ratshilengo, C. Sigauke, A. Bere, Short-Term Solar Power Forecasting Using Genetic Algorithms: An Application Using South African Data, Appl. Sci. 11 (9) (2021) 4214, https://doi.org/10.3390/app11094214.
[60] J.A. Ruiz-Arias, J. Dudhia, C.A. Gueymard, A simple parameterization of the short-wave aerosol optical properties for surface direct and diffuse irradiances assessment in a numerical weather model, Geosci. Model Dev. (2014), https://doi.org/10.5194/gmd-7-1159-2014.
[61] V. Salamalikis, I. Vamvakas, P. Blanc, A. Kazantzidis, Ground-based validation of aerosol optical depth from CAMS reanalysis project: An uncertainty input on direct normal irradiance under cloud-free conditions, Renew. Energy 170 (2021) 847–857.
[62] W. Sawadogo, J. Bliefernicht, B. Fersch, S. Salack, S. Guug, B. Diallo, Ogunjobi, O. Kehinde, G. Nacoulma, M. Tanu, S. Meilinger, H. Kunstmann, Hourly global horizontal irradiance over West Africa: A case study of one-year satellite- and reanalysis-derived estimates vs. In Situ Measurements, Renewable Energy (2023) 119066, https://doi.org/10.1016/j.renene.2023.119066.
[63] W. Sawadogo, J. Bliefernicht, B. Fersch, S. Salack, S. Guug, Ogunjobi, O. Kehinde, S. Meilinger, H. Kunstmann, Global Horizontal Irradiance in West Africa: Evaluation of the WRF-Solar Model in Convective Permitting Mode with Ground Measurements, J. Appl. Meteorol. Climatol. (2023), https://doi.org/10.1175/JAMC-D-22-0186.1.
[64] D. Yang, J.M. Bright, Worldwide validation of 8 satellite-derived and reanalysis solar radiation products: A preliminary evaluation and overall metrics for hourly data over 27 years, Solar Energy 210 (2020) 3–19.
[65] M.G. Schultz, C. Betancourt, B. Gong, F. Kleinert, M. Langguth, L.H. Leufen, A. Mozaffari, S. Stadtler, Can deep learning beat numerical weather prediction? Philos. Roy. Soc. A 379 (2194) (2021) 10–1098.
[66] G.L. Schuster, O. Dubovik, B.N. Holben, Angstrom exponent and bimodal aerosol size distributions, J. Geophys. Res. Atmos. 111 (D7) (2006).
[67] I. Sosa-Tinoco, M.A. Prósper, G. Miguez-Macho, Development of a solar energy forecasting system for two real solar plants based on WRF Solar with aerosol input and a solar plant model, Sol. Energy 240 (2022) 329–341, https://doi.org/10.1016/j.solener.2022.05.049.
[68] G. Thompson, T. Eidhammer, A Study of Aerosol Impacts on Clouds and Precipitation Development in a Large Winter Cyclone, J. Atmos. Sci. 71 (10) (2014) 3636–3658, https://doi.org/10.1175/JAS-D-13-0305.1.
[69] T. Vandal, E. Kodra, A.R. Ganguly, Intercomparison of machine learning methods for statistical downscaling: The case of daily and extreme precipitation, Theor. Appl. Climatol. 137 (1–2) (2019) 557–570, https://doi.org/10.1007/s00704-018-2613-3.
[70] C. Voyant, P. Lauret, G. Notton, J.-L. Duchaud, L. Garcia-Gutierrez, G. A. Faggianelli, Complex-valued time series based solar irradiance forecast, J. Renewable Sustainable Energy 14 (6) (2022) 066502, https://doi.org/10.1063/5.0128131.

[71] C. Voyant, G. Notton, S. Kalogirou, M.-L. Nivet, C. Paoli, F. Motte, A. Fouilloy, Machine learning methods for solar radiation forecasting: A review, Renew. Energy 105 (2017) 569–582, https://doi.org/10.1016/j.renene.2016.12.095.
[72] P. Wang, R. van Westrhenen, J.F. Meirink, S. van der Veen, W. Knap, Surface solar radiation forecasts by advecting cloud physical properties derived from Meteosat Second Generation observations, Sol. Energy 177 (2019) 47–58, https://doi.org/10.1016/j.solener.2018.10.073.
[73] Y. Xie, M. Sengupta, J. Dudhia, A Fast All-sky Radiation Model for Solar applications (FARMS): Algorithm and performance evaluation, Sol. Energy 135 (2016) 435–445.
[74] D. Yang, A correct validation of the National Solar Radiation Data Base (NSRDB), Renew. Sustain. Energy Rev. 97 (2018) 152–155, https://doi.org/10.1016/j.rser.2018.08.023.
[75] D. Yang, Making reference solar forecasts with climatology, persistence, and their optimal convex combination, Sol. Energy 193 (2019) 981–985.
[76] D. Yang, S. Alessandrini, J. Antonanzas, F. Antonanzas-Torres, V. Badescu, H. G. Beyer, R. Blaga, J. Boland, J.M. Bright, C.F.M. Coimbra, M. David, A. Frimane, C.A. Gueymard, T. Hong, M.J. Kay, S. Killinger, J. Kleissl, P. Lauret, E. Lorenz, J. Zhang, Verification of deterministic solar forecasts, Sol. Energy 210 (2020) 20–37, https://doi.org/10.1016/j.solener.2020.04.019.
[77] J. Yang, M. Sengupta, P.A. Jiménez, J.-H. Kim, Y. Xie, Evaluating WRF-Solar EPS cloud mask forecast using the NSRDB, Sol. Energy 243 (2022) 348–360, https://doi.org/10.1016/j.solener.2022.08.003.
[78] E. Zhandire, Predicting clear-sky global horizontal irradiance at eight locations in South Africa using four models, J. Energy Southern Africa 28 (4) (2017) 77–86.
[79] Zhang, J., Hodge, B.-M., Florita, A., Lu, S., Hamann, H. F., & Banunarayanan, V. (2013). *Metrics for evaluating the accuracy of solar power forecasting*. National Renewable Energy Lab.(NREL), Golden, CO (United States).